Supplement of Geosci. Model Dev., 16, 5627–5652, 2023
https://doi.org/10.5194/gmd-16-5627-2023-supplement

Geoscientific Model Development
Open Access
EGU

Supplement of

Modeling sensitivities of thermally and hydraulically driven ice stream surge cycling

Kevin Hank et al.

Correspondence to: Kevin Hank (khank@mun.ca)

S1 GSM - Details of different model aspects

S1.1 Climate forcing

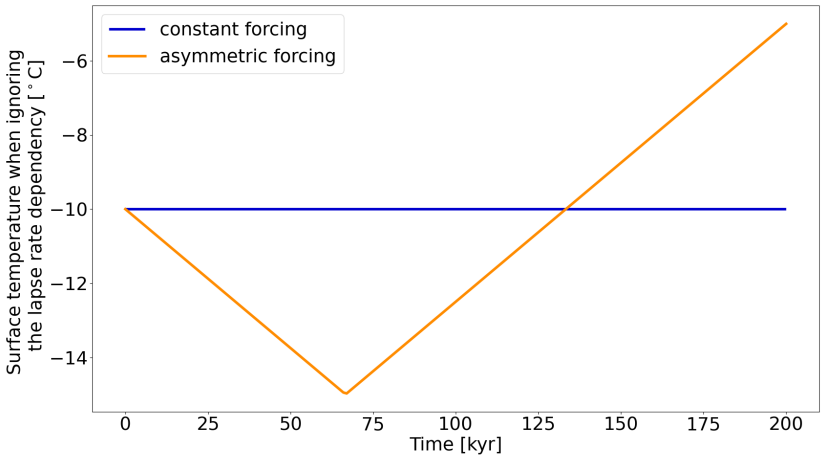

Figure S1. Constant and asymmetric temperature forcing in the GSM. The coldest temperature is reached at 66.7 kyr. For the case shown here, the surface temperature constant is set to rTsurf$= -10^{\circ}$C (Table 1). All model runs within this paper use the asymmetric forcing.

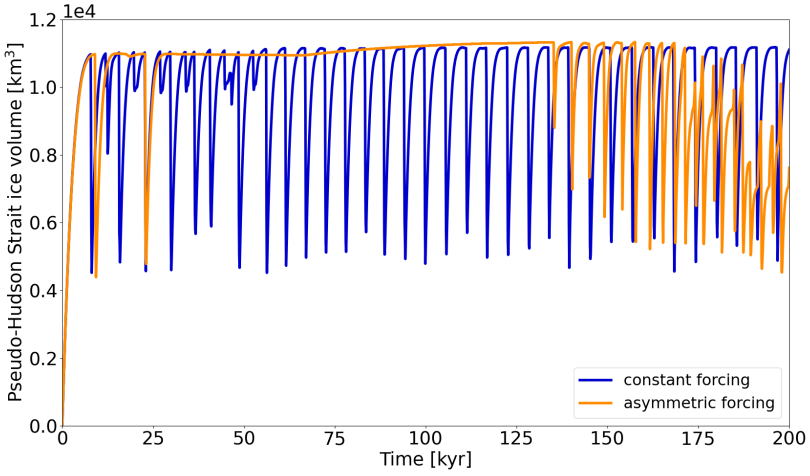

Figure S2. Pseudo-Hudson Strait ice volume for a constant and asymmetric temperature forcing in the GSM (Fig. S1). This plot shows parameter vector 1 with a horizontal grid resolution of 25 km.

S1.2 SSA activation velocities

Setup	number of surges	mean duration	mean period	mean pseudo-Hudson Strait ice volume change
reference setup	180 ± 100	1.1 ± 0.5 kyr	0.3 ± 0.1 kyr	$1.7 \pm 0.2 \cdot 10^3$ km^3
$v_{\mathrm{SIA,crit}} = 20$ m yr^{-1}	-3.7 ± 7.0	3.2 ± 6.4	1.5 ± 2.1	3.2 ± 2.4
$v_{\mathrm{SIA,crit}} = 40$ m yr^{-1}	-5.5 ± 5.4	6.1 ± 6.8	2.4 ± 5.7	3.5 ± 9.0
SSA everywhere	7.3 ± 24.8	1.7 ± 27.6	-9.3 ± 14.1	-17.7 ± 29.7

Table S1. Percentage differences (except first row) of surge characteristics between the GSM reference setup (first row) and runs with different SSA activation velocities at 3.125 km. By default, the SSA is activated once the SIA velocity exceeds $v_{\mathrm{SIA,crit}} = 30$ m yr^{-1}. No runs crashed and all runs had more than 1 surge. The first 20 kyr of each run are treated as a spin-up interval and are not considered in the above.

S1.3 Parameter vectors

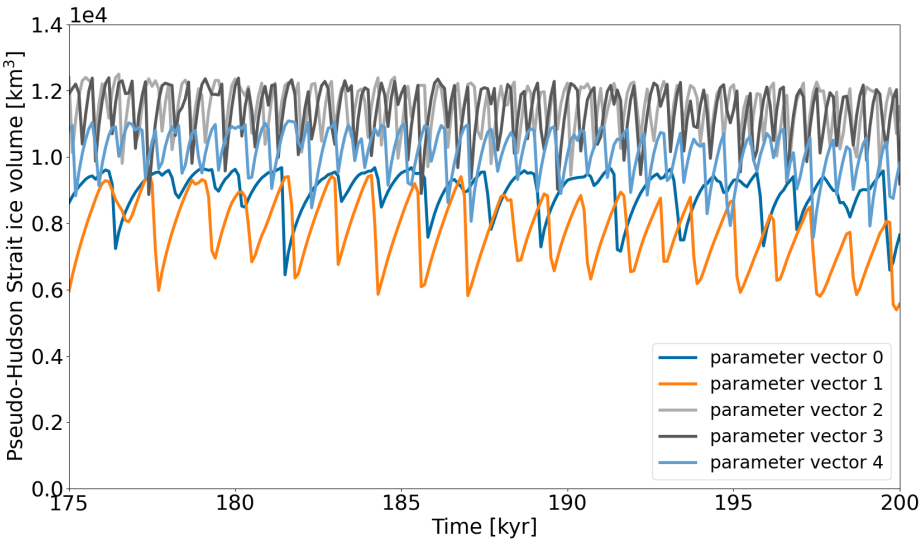

Figure S3. Pseudo-Hudson Strait ice volume for the last 25 kyr of all 5 GSM parameter vectors when using the reference setup. Note that only the last 25 kyr are shown for better visibility of the individual oscillation pattern.

S1.4 Bed properties

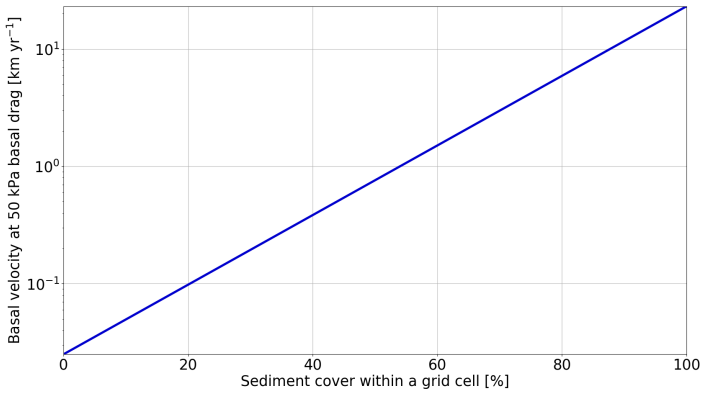

Figure S4. Basal velocity at 50 kPa basal drag for variable sediment cover and a power-law exponent of 3 (n_b in Table 1).

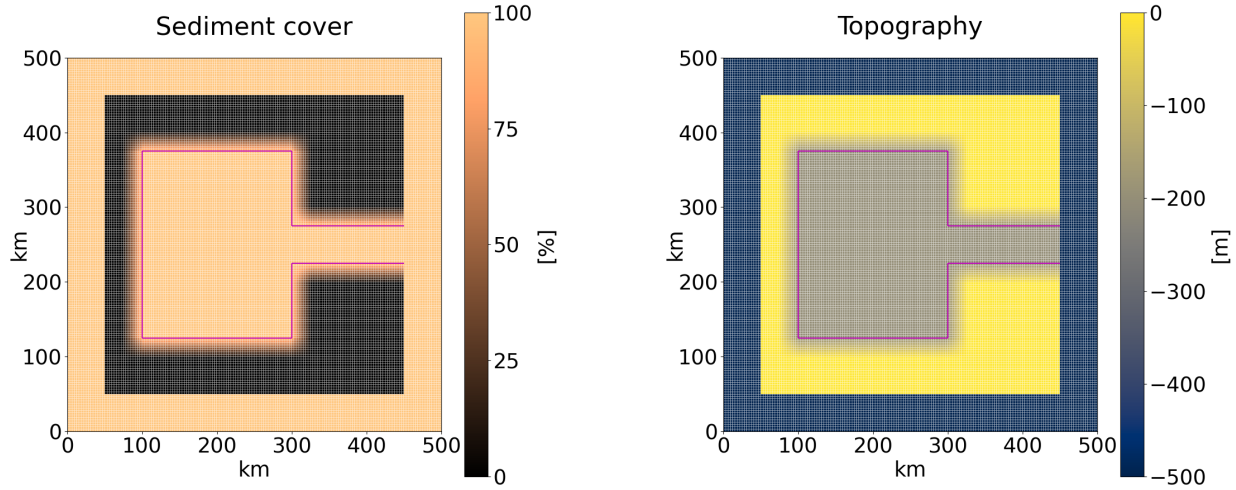

(a) (b)

Figure S5. Sediment cover and topography map for a 25 km wide transition zone at 3.125 km horizontal grid resolution. The transition zones for topography and sediment cover are at the same locations. The magenta line outlines the 100 % soft-bedded pseudo-Hudson Bay and Hudson Strait.

The effects of an abrupt transition from hard bedrock (0 % sediment cover) to soft sediment (100 % sediment cover) are examined by adding a smooth transition zone (Fig. S5 a)). Two widths of this transition zone (25 km and 3.125 km) are investigated. The basal velocity (or more precisely the sliding coefficient C in Eq. (6b)) then depends on the sediment cover

within a grid cell (Fig. S4). In the experiments with a non-flat topography, the bed of the pseudo-Hudson Bay and Hudson Strait is placed 200 m and the surrounding ocean 500 m below the sea level (Fig. S5 b). The topographic transition zones (25 km and 3.125 km wide) align with the sediment transition zones.

S1.5 Weighting function of the adjacent minimum basal-temperature

A weighting function takes into account the adjacent minimum basal-temperature for the basal-sliding temperature ramp.

$$T_{\mathrm{bp,I}} = W_{\mathrm{Tb,min}} \cdot \min\left[T_{\mathrm{bp,L}}, T_{\mathrm{bp,R}}\right] + T_{\mathrm{bp,I}} \cdot \left(1 - W_{\mathrm{Tb,min}}\right), \tag{S1}$$

where $T_{\mathrm{bp,I}}$ is the basal-temperature with respect to the pressure-melting point at the grid cell interface, and $T_{\mathrm{bp,L}}$ and $T_{\mathrm{bp,R}}$ are the basal-temperatures with respect to the pressure-melting point at the adjacent grid cell centers. Note that $T_{\mathrm{bp,Im,L}}$ and $T_{\mathrm{bp,Im,R}}$ instead of $T_{\mathrm{bp,L}}$ and $T_{\mathrm{bp,R}}$ are used when calculating $T_{\mathrm{bp,I}}$ according to TpmTrans (Eq. (18)). In this way, the additional heat T_{add} is still considered even when $W_{\mathrm{Tb,min}} = 1$.

S2 PISM - Details of different model aspects

S2.1 Input fields

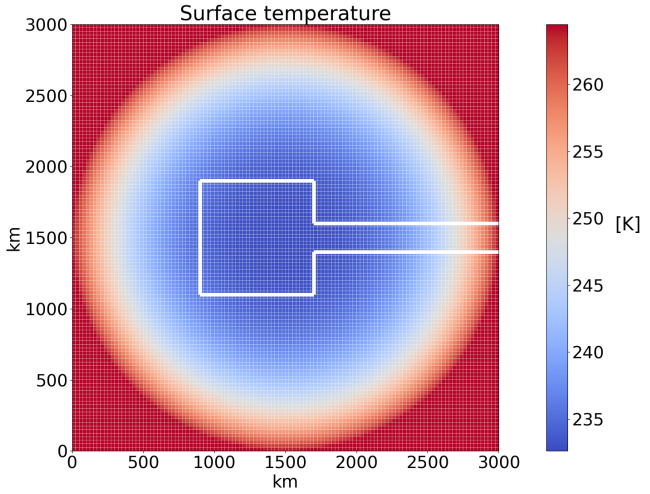

Figure S6. PISM surface temperature input field for parameter vector 1. The corresponding parameter values of T_{min} and S_{t} are 232.60 K and $9.45 \cdot 10^{-9}$ K km^{-3}, respectively. Thick white lines outline the simplified soft-bedded pseudo-Hudson Bay/Hudson Strait area. The horizontal grid resolution is 25x25 km.

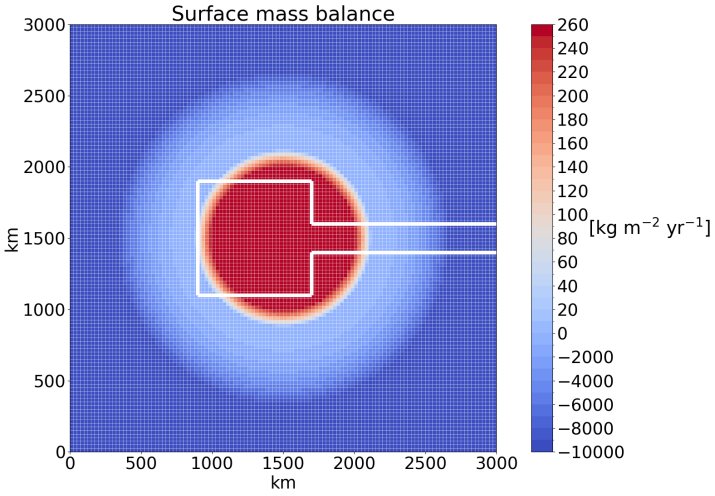

Figure S7. PISM surface mass balance input field for parameter vector 1. The corresponding parameter values of $B_{\max}$ and S_{b} are $408.81\ \mathrm{kg\ m^{-2}\ yr^{-1}}$ and $4.55 \cdot 10^{-12}\ \mathrm{kg\ m^{-2}\ yr^{-1}\ km^{-5}}$, respectively. Thick white lines outline the simplified soft-bedded pseudo-Hudson Bay/Hudson Strait area. The horizontal grid resolution is $25\mathrm{x}25\ \mathrm{km}$.

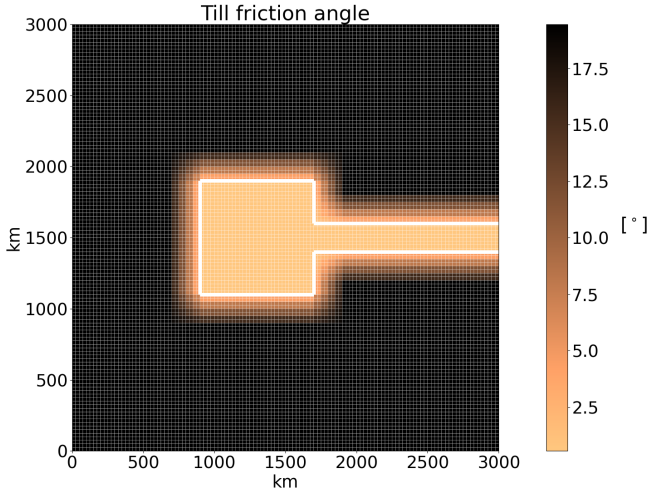

Figure S8. PISM till friction angle input field for parameter vector 1. The corresponding parameter values of $soft$ and $hard$ are $0.56°\mathrm{C}$ and $19.44°\mathrm{C}$, respectively. Magenta lines outline the simplified soft-bedded pseudo-Hudson Bay/Hudson Strait area. The horizontal grid resolution is $25\mathrm{x}25\ \mathrm{km}$.

S2.2 Parameter vectors

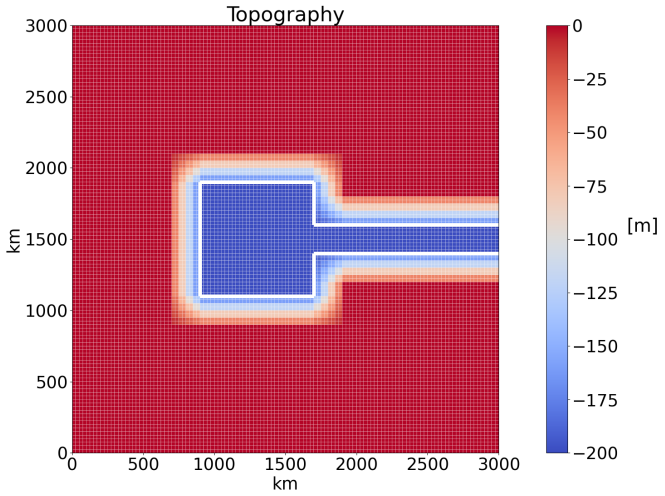

Figure S9. PISM topography input field (same for all parameter vectors). The white lines outline the simplified soft-bedded pseudo-Hudson Bay/Hudson Strait area. The horizontal grid resolution is 25x25 km.

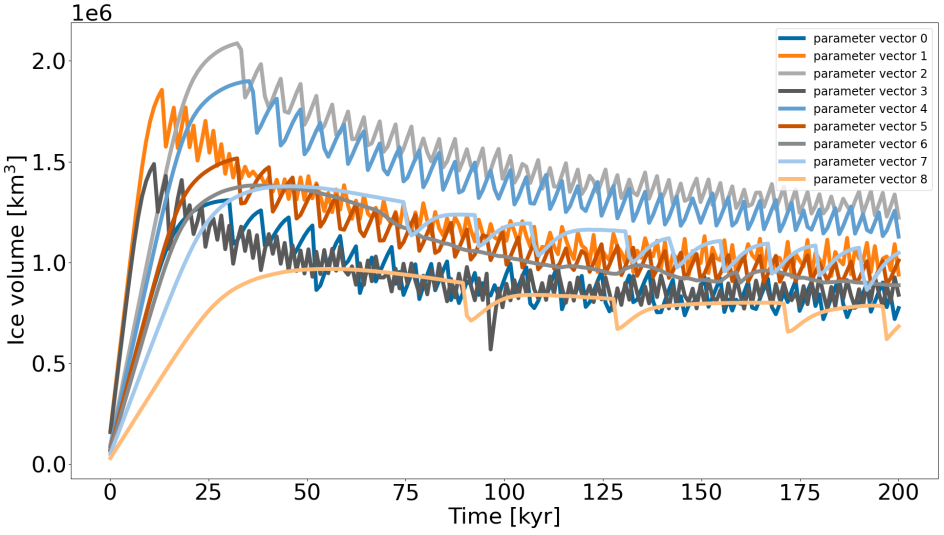

Figure S10. Ice volume in the eastern half of the pseudo-Hudson Bay and the pseudo-Hudson Strait for all 9 PISM parameter vectors when using the reference setup.

S2.3 Bed properties

In PISM, oscillatory behavior only occurs for small yield stresses τ_c (Eq. (15)). This can be achieved by either a small till friction angle Φ or low effective-pressure on the till (N_{till}) (Bueler and Van Pelt, 2015). N_{till} is given by

$$N_{\text{till}} = \min\left\{P_0, N_0 \left(\frac{\delta_e P_0}{N_0}\right)^s 10^{\left(\frac{e_0}{C_c}\right)(1-s)}\right\}, \tag{S2}$$

where P_0 is the ice overburden pressure, $N_0 = 1$ kPa is the reference effective-pressure, $e_0 = 0.69$ the void ratio at N_0, $C_c = 0.12$ the dimensionless coefficient of compressibility, δ_e the effective fraction of the overburden pressure, P_0 the ice overburden pressure, and s the ratio $\frac{W_{\text{till}}}{W_{\text{till}}^{\max}}$ (Tulaczyk et al., 2000; Bueler and Van Pelt, 2015). W_{till} and $W_{\text{till}}^{\max} = 2$ m are the effective and maximum thickness of water in the till, respectively. The values listed here are the PISM defaults. C_c is on the lower end of measured values (Tulaczyk et al., 2000) with significantly larger (up to 17) values reported (Sauer et al., 1993; Mitchell and Soga, 2005). e_0 can vary between 0.45 (Tulaczyk et al., 2000) and approximately 4 (Fig. 10.2 in Mitchell and Soga, 2005). The default value of δ_e is based on Greenland and Antarctic model runs, but δ_e is generally considered as a tuning parameter to match observed surface velocities, which are not available in a paleo context (Andy Aschwanden, personal communication).

When only changing the till friction angle (Eq. (15)), oscillations do not occur unless $\Phi < 1°$ (Fig. S13). This is well below the measured values of about 10 to 40° (K.M. Cuffey and W.S.B. Paterson., 2010). However, similar oscillatory results are obtained for till friction angles between 5 and 10° when slightly adjusting the values of $C_c = 0.2$, $e_0 = 0.6$, and $\delta_e = 0.01$ to favor sliding (compare Fig. S11 and S12). These values are all well within the ranges set by laboratory measurements.

S2.4 Maximum magnitude of basal ice velocity

Small till friction angles (0.5 to 1.0°) lead to slippery beds and high maximum basal-sliding velocities (up to ~ 600 km yr^{-1}) for a small number of time steps in some runs. A maximum of 7 out of 2000 time steps exceeds 50 km yr^{-1} (parameter vector 1 in Fig. S11). While observed velocities can reach several hundreds of meters per day for short periods (K.M. Cuffey and W.S.B. Paterson. (2010), e.g., 300 m d^{-1} = 109.5 km yr^{-1}), high modeled velocities might lead to instabilities in the numerical matrix solver. Therefore, we set an upper limit of 40 km yr^{-1} for the SSA velocity.

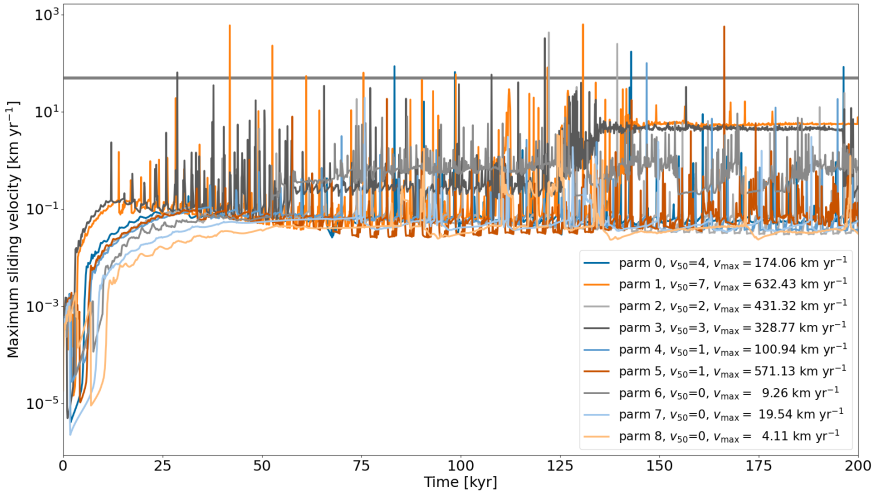

Figure S11. Maximum sliding velocity (max(max(abs($\boldsymbol{u}$)), max(abs($\boldsymbol{v}$)))) at each time step (100 yr interval) within the whole model domain for all 9 parameter vectors using PISM without an upper limit for the SSA velocity. The black horizontal line marks 50 km yr^{-1} and v_{50} indicates the number of time steps exceeding this velocity. $v_{\max}$ is the highest maximum sliding velocity in a run.

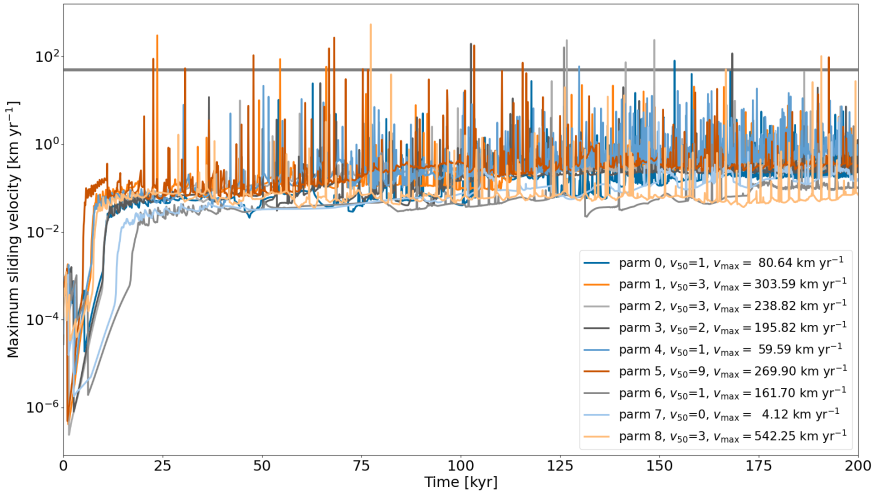

Figure S12. Maximum sliding velocity (max(max(abs($\boldsymbol{u}$)), max(abs($\boldsymbol{v}$)))) at each time step (100 yr interval) within the whole model domain for 9 parameter vectors with till friction angles between 5 and 10° and values of $C_c = 0.2$, $e_0 = 0.6$, and $\delta_e = 0.01$ using PISM without an upper limit for the SSA velocity. The black horizontal line marks 50 km yr^{-1} and v_{50} indicates the number of time steps exceeding this velocity. v_{max} is the highest maximum sliding velocity in a run.

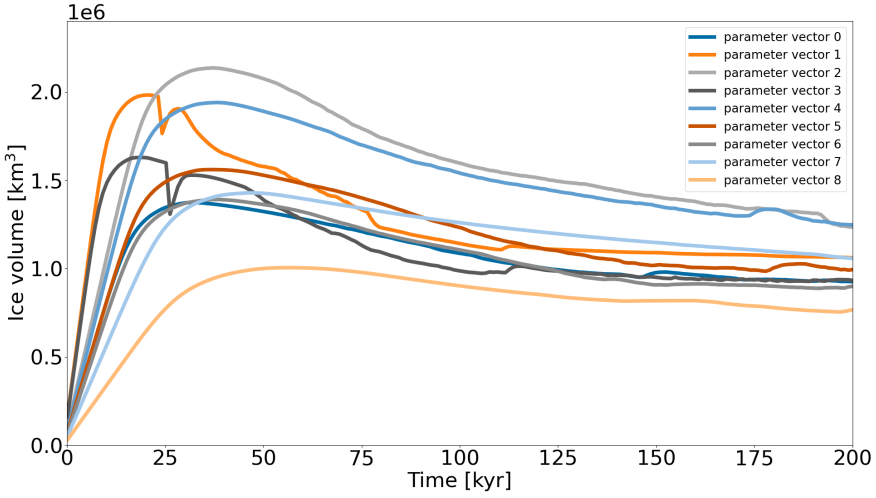

Figure S13. Ice volume in the eastern half of the pseudo-Hudson Bay and the pseudo-Hudson Strait for all 9 PISM parameter vectors when using the reference setup but a soft-bed till friction angle of 1°.

S2.5 Ice volume - pseudo-Hudson Strait vs. surge-affected area

During a surge, ice from the pseudo-Hudson Bay and areas surrounding the pseudo-Hudson Strait is rapidly transported into the mostly ice-free pseudo-Hudson Strait. Consequently, the ice sheet extends further to the East (increasingly stronger melting), covering almost the entire pseudo-Hudson Strait area. Due to the complex interaction between ice transport and melting area, times of minimum ice volume over the area most affected by the pseudo-Hudson Strait surge (eastern half of the pseudo-Hudson Bay and the pseudo-Hudson Strait, e.g., Fig. 5 and video 06 of Hank (2023)) correspond to maxima in the pseudo-Hudson Strait ice volume for most surges (grey lines in Fig. S14). However, some ice volume minima do not align with a maximum of the pseudo-Hudson Strait ice volume (red lines in Fig. S14). This inconsistency hampers the detection of surges when using the pseudo-Hudson Strait ice volume and can lead to flawed statistics. To avoid this issue, we use the ice volume in the surge-affected area, for which surges appear as minima, for all PISM results. A comparison between PISM results based on the pseudo-Hudson Strait and the surge-affected area is shown in Fig. S15. Note that we only consider the eastern half of the pseudo-Hudson Bay because some runs also show surges on the Western side of the ice sheet (e.g., 50 km run in video 09 of Hank (2023)).

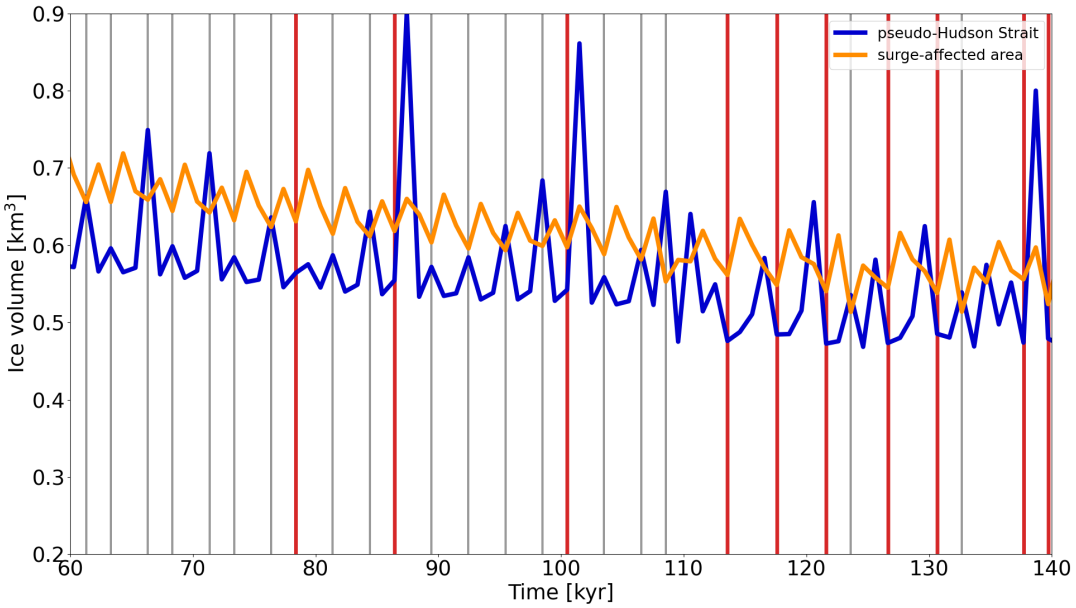

Figure S14. Normalized pseudo-Hudson Strait and surge-affected area (eastern half of the pseudo-Hudson Bay and the pseudo-Hudson Strait) ice volume for parameter vector 1 using PISM. For most surges, the minimum ice volume over the surge-affected area aligns with a maxima in the pseudo-Hudson Strait ice volume (grey lines). This is, however, not true for all surges (thick red lines) and can lead to flawed statistics. See also video 06 of Hank (2023).

S3 Run analysis approach

For both models, we use the Python module *scipy* (version 1.5.2 on GSM cluster and 1.7.0 on PISM cluster, different versions due to the availability on computational clusters) and its built-in function *scipy.signal.find_peaks* on the ice volume output to determine the surge characteristics. The surge duration and ice volume change during a surge are determined by the functions *scipy.signal.peak_widths* and *scipy.signal.peak_prominences*, respectively. The Python analysis scripts are provided as supplementary material.

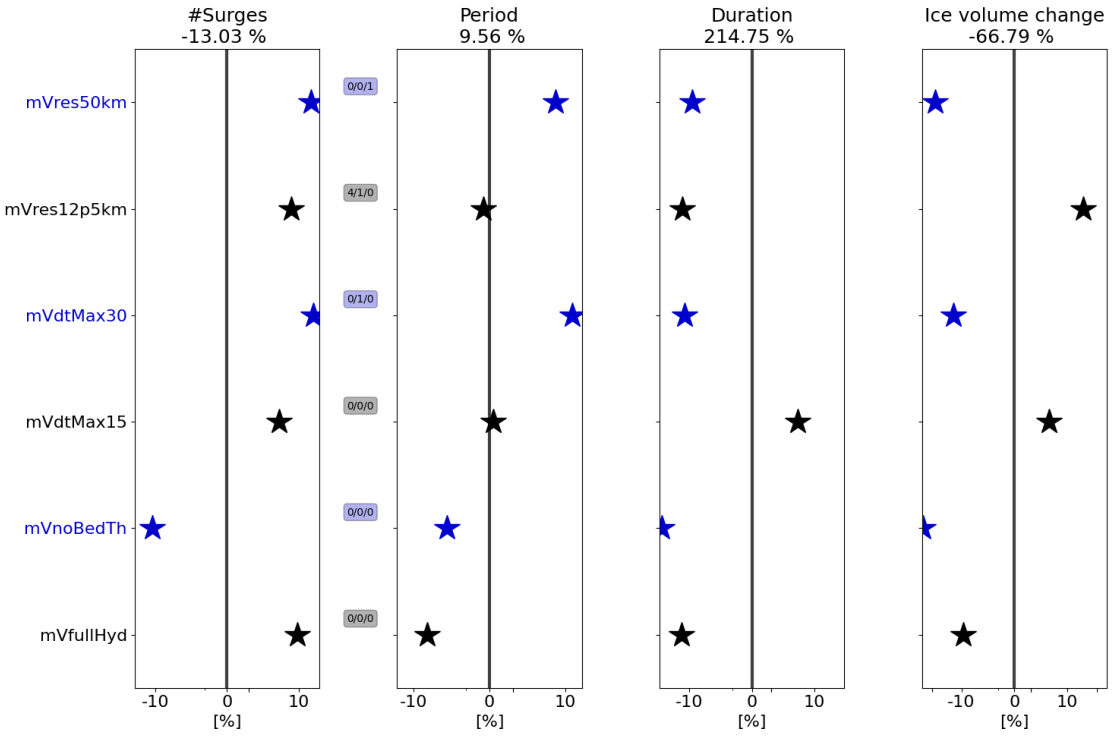

Figure S15. Differences in the percentage differences of the mean surge characteristics (between comparison and reference setup) when using the ice volume of the surge-affected area (eastern half of the pseudo-Hudson Bay and the pseudo-Hudson Strait) compared to only the pseudo-Hudson Strait ice volume. A positive difference indicates a larger change for the analysis based on the pseudo-Hudson Strait ice volume. The different colors were added for visual alignment of the individual model setups. The 3 small numbers between the first two columns represent the number of crashed runs (nC), the number of runs without a surge (nS0), and the number of runs with only one surge (nS1), respectively. The first 20 kyr of each run are treated as a spin-up interval and are not considered in the above. The percentages in the titles of each subplot represent the percentage differences in the surge characteristics of the reference runs. For example, the mean number of surges based on the pseudo-Hudson Strait ice volume is ~ 13 % smaller than for the ice volume of the surge-affected area. Note that the surge threshold is $4 \cdot 10^4$ km^3 when using the surge-affected area ice volume and $0.5 \cdot 10^4$ km^3 for the pseudo-Hudson Strait ice volume (~ 5 % of mean ice volume across all runs). The x-axis is logarithmic. Further details of each individual experiments are provided in Fig. 6.

Temporal resolution of output time series

The standard output time steps in the GSM and PISM are 0.1 and 1 kyr, respectively. Note that these time steps might not exactly capture the minimum ice volume but are generally a good compromise between storage requirements and temporal resolution (e.g., Fig. S16 and S17).

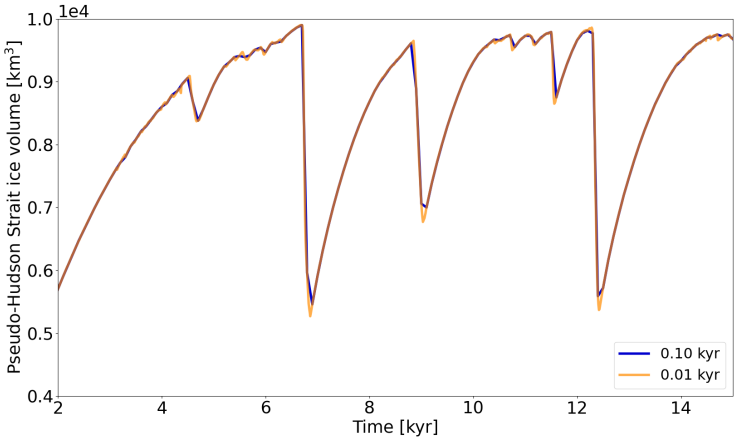

Figure S16. Pseudo-Hudson Strait ice volume of a GSM model run (parameter vector 1) with different output time steps. The horizontal grid resolution is 3.125 km.

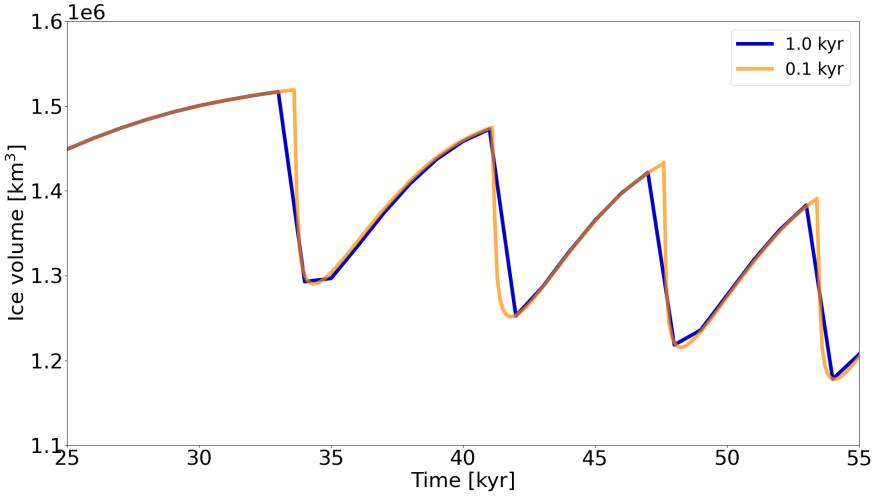

Figure S17. Ice volume in the surge-affected area (eastern half of the pseudo-Hudson Bay and the pseudo-Hudson Strait) of a PISM model run (parameter vector 5) with different output time steps. The horizontal grid resolution is 25 km.

S4 RMSE and mean bias

The RMSE and mean bias values presented throughout the paper are calculated according to the following equations

$$rmse = \sqrt{\frac{\sum_{\mathrm{t}=0}^{t_{\max}} (x_{\mathrm{t}} - b_{\mathrm{t}})^2}{N}} \cdot \frac{100}{b_{\mathrm{m}}}, \text{ and} \tag{S3}$$

$$mean\ bias = \frac{\sum_{\mathrm{t}=0}^{t_{\max}} (x_{\mathrm{t}} - b_{\mathrm{t}})}{N} \cdot \frac{100}{b_{\mathrm{m}}}, \tag{S4}$$

where x_{t} and b_{t} are the (pseudo-Hudson Strait) ice volume values at time t of the comparison setup and reference setup, respectively. $t_{\max}$ is the maximum time, N the number of time steps, and b_{m} the mean of the reference setup time series. These values are then averaged over all 5 parameter vectors. Crashed runs are excluded from the averaging process.

S5 Comparison between different model setups

The analysis to compare the different model setups follows

1. run 1 parameter vector with the reference setup (Table 2)
2. calculate the surge characteristics for this reference run (s_{ref})
3. re-run the same parameter vector for one of the comparison setups (Sec. 2.1.3 and 2.2.4)
4. calculate the surge characteristics for the comparison run (s_{comp})
5. calculate the differences in surge characteristics between the reference run and comparison run expressed as percentage differences from the reference run (positive for increase compared to the value of the reference run): $p = \frac{s_{\mathrm{comp}} - s_{\mathrm{ref}}}{s_{\mathrm{ref}}} \cdot 100$
6. repeat steps 1) to 5) for all parameter vectors (5 for the GSM, 9 for PISM)
7. the values shown in the tables and figures are the mean and standard deviation of all percentage differences for each surge characteristic

Percentage differences for crashed comparison runs are not considered for the final average and runs with less than 2 surges require special treatment. In these cases, the period is set to a NaN value, leading to a NaN difference between that particular run and the corresponding reference run. We use Numpys *numpy.nanmean()* and *numpy.nanstd()* to ignore these NaN values when averaging over all parameter vectors. Similarly, all surge characteristics except for the number of surges are set to NaN values for runs with no surges at all. Note that the values for the reference setup stated in the tables are the mean and standard deviation of the actual surge characteristics of all reference runs, not percentage differences.

S6 Minimum numerical error estimates

S6.1 GSM

S6.1.1 Minimum numerical error estimates at 12.5 km

Metric	original $12.5\ \mathrm{km}$ runs	stricter numerical convergence [% difference]	stricter numerical convergence with increased maximum iterations [% difference]
#Surges	81 ± 42	2.3 ± 8.5	$\mathbf{2.8 \pm 9.2}$
mean period	2.3 ± 0.8 kyr	$\mathbf{-2.1 \pm 7.5}$	-1.5 ± 9.3
mean duration	0.6 ± 0.2 kyr	-1.4 ± 9.4	$\mathbf{2.6 \pm 14.2}$
mean pseudo-Hudson Strait ice volume change	$2.2 \pm 1.1 \cdot 10^3\ \mathrm{km}^3$	$\mathbf{20.9 \pm 53.0}$	-5.1 ± 12.2

Table S2. Percentage differences (except first column) of surge characteristics between GSM runs with regular and stricter numerical convergence and increased maximum iterations for the ice dynamics loops at $12.5\ \mathrm{km}$. The values represent the average of 5 parameter vectors. No runs crashed and all runs had more than 1 surge. The first 20 kyr of each run are treated as a spin-up interval and are not considered in the above. The bold numbers mark the largest MNEE for each surge characteristic.

S6.1.2 Adding surface temperature noise

Metric	reference setup	± 0.1°C noise	± 0.5°C noise
#Surges	180 ± 100	-4.0 ± 4.3	-4.1 ± 7.0
mean period	1.1 ± 0.5 kyr	4.8 ± 5.3	3.8 ± 6.8
mean duration	0.3 ± 0.1 kyr	1.3 ± 4.4	0.9 ± 4.3
mean pseudo-Hudson Strait ice volume change	$1.7 \pm 0.2 \cdot 10^3\ \mathrm{km}^3$	0.9 ± 4.1	2.1 ± 5.5
RMSE	-	8.0 ± 2.5	7.8 ± 2.1
Mean Bias	-	-0.1 ± 0.2	0.1 ± 0.0

Table S3. Percentage differences (except first column) of surge characteristics, pseudo-Hudson Strait ice volume RMSE and mean bias compared to the GSM reference setup for two different amplitudes of surface temperature noise. No runs crashed and all runs had more than 1 surge. The first 20 kyr of each run are treated as a spin-up interval for the surge characteristics (not the RMSE and mean bias).

S6.1.3 Implicit thermodynamics/ice dynamics coupling

Metric	reference setup	implicit coupling
#Surges	180 ± 100	1.1 ± 4.9
mean period	1.1 ± 0.5 kyr	-0.3 ± 5.3
mean duration	0.3 ± 0.1 kyr	-12.7 ± 9.5
mean pseudo-Hudson Strait ice volume change	$1.7 \pm 0.2 \cdot 10^3$ km^3	-25.1 ± 18.7
RMSE	-	7.3 ± 2.5
Mean Bias	-	1.8 ± 1.5

Table S4. Percentage differences (except first column) of surge characteristics, pseudo-Hudson Strait ice volume RMSE and mean bias compared to the GSM reference setup for implicit coupling between the thermodynamics and ice dynamics in the GSM. No runs crashed and all runs had more than 1 surge. The first 20 kyr of each run are treated as a spin-up interval for the surge characteristics (not the RMSE and mean bias).

S6.2 PISM

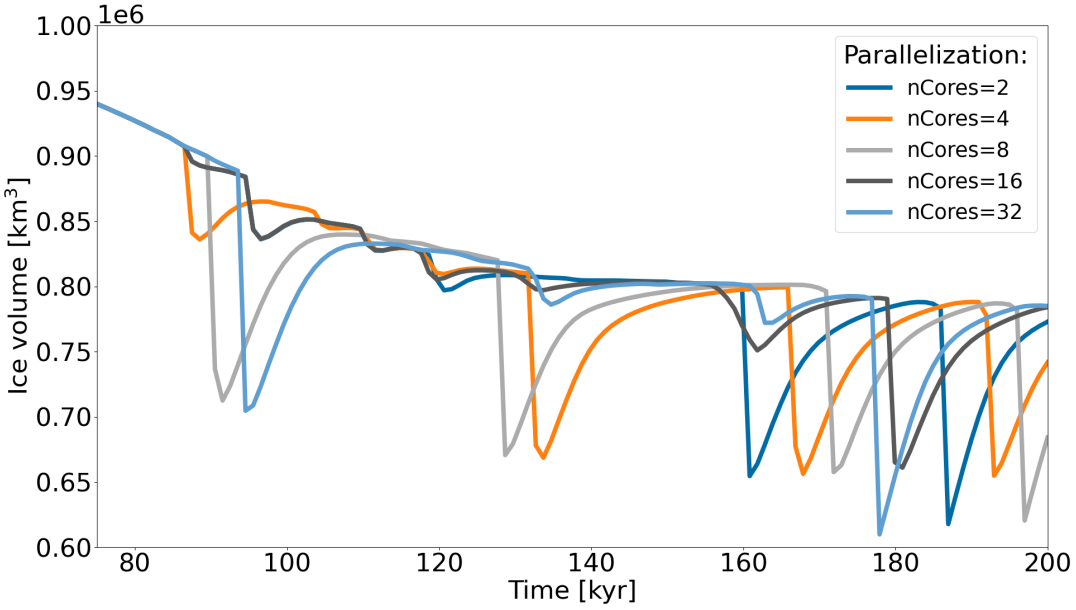

Figure S18. Ice volume in the eastern half of the pseudo-Hudson Bay and the pseudo-Hudson Strait for parameter vector 8 and different numbers of cores/processes using PISM.

S6.2.1 Relative tolerances

Setup	number of surges	mean period	mean duration	mean ice volume change	nC	nS1
25 km reference setup	35 ± 25	10 ± 10 kyr	3 ± 2 kyr	$1.1 \pm 0.3 \cdot 10^5$ km^3	0	0
nCores= 8, KSP= 10^{-10}	-10.7 ± 21.6	-1.8 ± 5.6	11.2 ± 32.8	5.3 ± 11.2	0	1
nCores= 16, KSP= 10^{-10}	-4.7 ± 22.4	-2.7 ± 4.8	0.1 ± 9.3	-0.4 ± 5.1	0	1
nCores= 32, KSP= 10^{-10}	-10.5 ± 28.7	-3.7 ± 6.2	-1.2 ± 12.4	1.2 ± 7.2	4	1
nCores= 8, KSP= 10^{-10}, PIC= 10^{-7}	8.3 ± 11.8	-28.6 ± 17.4	-17.1 ± 35.2	9.0 ± 21.5	6	0
nCores= 16, KSP= 10^{-10}, PIC= 10^{-7}	98.1 ± 135.9	-22.5 ± 10.1	-14.4 ± 24.6	15.7 ± 54.4	5	0
nCores= 32, KSP= 10^{-10}, PIC= 10^{-7}	83.8 ± 125.1	-18.2 ± 11.6	-13.9 ± 25.7	23.2 ± 56.4	5	0

Table S5. Percentage differences (except first row) of surge characteristics compared to the PISM reference setup with different numbers of cores and adjusted relative tolerances for the Picard iteration in the calculation of the vertically-averaged effective viscosity (PIC, default is 10^{-4}) and the Krylov linear solver used at each Picard iteration (KSP, default is 10^{-7}). The values represent the average of 9 parameter vectors. Crashed runs (nC) are not considered and runs with just one surge (nS1) are ignored when calculating the change in mean period. The first 20 kyr of each run are treated as a spin-up interval and are not considered in the above. Note that more than 50 % of all runs with KSP= 10^{-10} and PIC= 10^{-7} did not finish within the time limit set by the computational cluster and are considered as crashed runs (nC). A direct comparison of runs with these tolerances can be found in Fig. S19. Note that all test runs without preconditioning (removes processor-number-dependence of results) crashed during the spin-up phase and long before the first surge occurs.

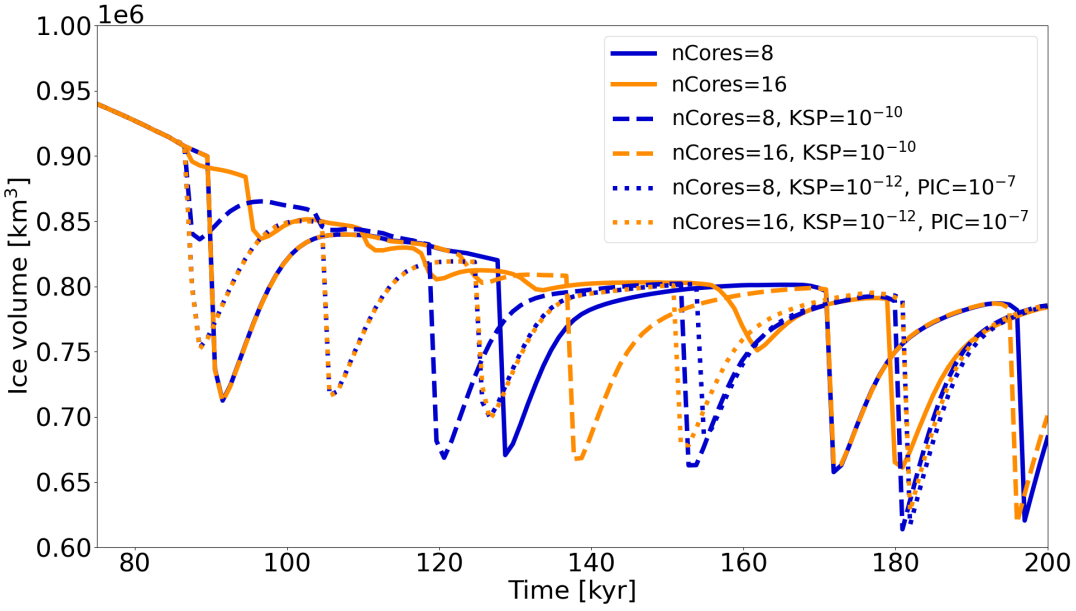

Figure S19. Ice volume in the eastern half of the pseudo-Hudson Bay and the pseudo-Hudson Strait for parameter vector 8 and different number of cores/processes using PISM with different relative tolerances for the Picard iteration in the calculation of the vertically-averaged effective viscosity (PIC, default is 10^{-4}) and the Krylov linear solver used at each Picard iteration (KSP, default is 10^{-7}.

S6.2.2 Adding surface temperature noise

Metric	reference setup	$\pm 0.1^\circ$C noise	$\pm 0.5^\circ$C noise
#Surges	35 ± 25	-12.4 ± 24.2	-12.0 ± 25.2
mean period	10 ± 10 kyr	-5.6 ± 8.0	-4.0 ± 8.8
mean duration	3 ± 2 kyr	11.5 ± 37.9	2.0 ± 12.9
mean pseudo-Hudson Strait ice volume change	$1.1 \pm 0.3 \cdot 10^5$ km^3	1.9 ± 15.9	2.5 ± 8.1
RMSE	-	4.1 ± 3.5	4.3 ± 2.6
Mean Bias	-	-0.8 ± 1.9	0.1 ± 0.3
nS1	0	1	1

Table S6. Percentage differences (except first column) of surge characteristics, ice volume RMSE and mean bias compared to the PISM reference setup for two different amplitudes of surface temperature noise. No runs crashed and all runs showed at least 1 surge. Runs with just one surge (nS1) are ignored when caluclating the change in mean period. The first 20 kyr of each run are treated as a spin-up interval for the surge characteristics (not the RMSE and mean bias).

S7 Sensitivity experiments with a significant effect

S7.1 Bed thermal model

Metric	reference setup	20 m deep (1 layer) bed thermal model
number of surges	180 ± 100	-31.6 ± 5.6
mean period	1.1 ± 0.5 kyr	60.2 ± 22.4
mean duration	0.3 ± 0.1 kyr	65.2 ± 24.5
mean pseudo-Hudson Strait ice volume change	$1.7 \pm 0.2 \cdot 10^3$ km^3	49.6 ± 14.6
RMSE	-	10.4 ± 2.2
Mean Bias	-	-2.3 ± 1.7

Table S7. Percentage differences (except first column) of surge characteristics, pseudo-Hudson Strait ice volume RMSE and mean bias compared to the GSM reference setup for runs with only one bed thermal layer (20 m deep). No runs crashed and all runs had more than 1 surge. The first 20 kyr of each run are treated as a spin-up interval for the surge characteristics (not the RMSE and mean bias).

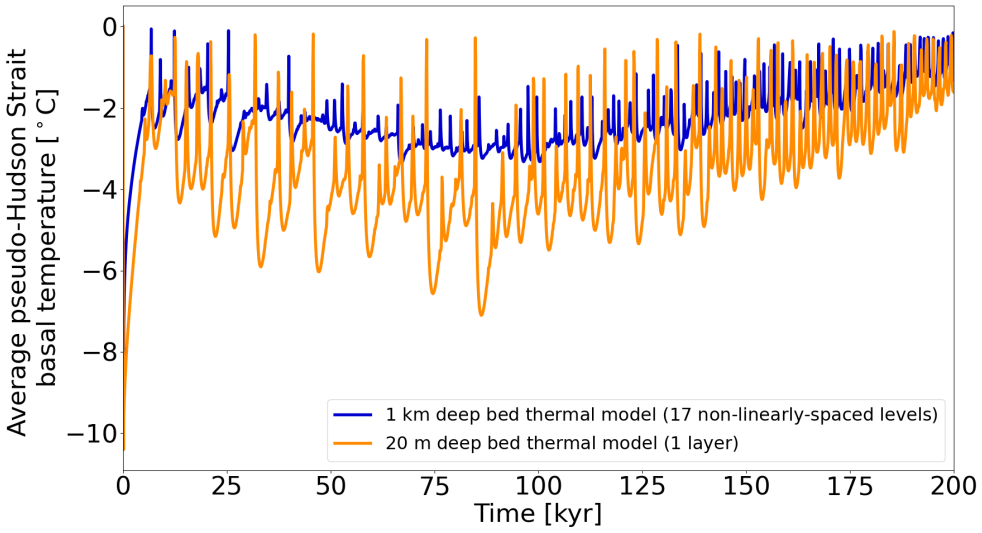

Figure S20. Average pseudo-Hudson Strait basal ice temperature with respect to the pressure-melting point for parameter vector 1 with a 20 m and 1 km deep bed thermal model (17 non-linearly-spaced levels) using the GSM. The horizontal grid resolution is 3.125 km.

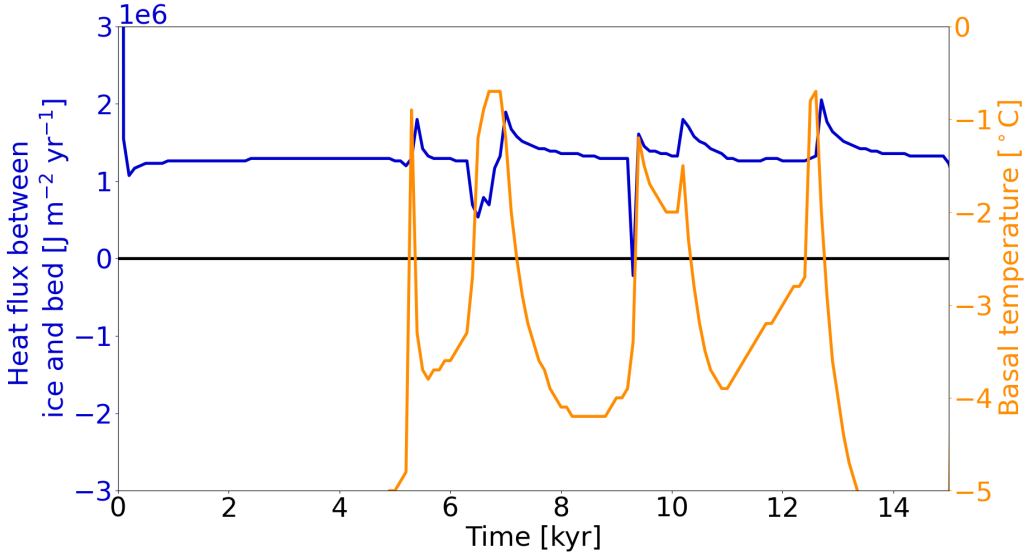

Figure S21. Heat flux at the base of the ice sheet (positive from bed into ice) and basal ice temperature for a grid cell in the center of the pseudo-Hudson Strait (grid cell center at $x = 376.5625$ km and $y = 248.4375$ km, white star in Fig. 1) and parameter vector 1 with only one bed thermal layer (20 m deep) using the GSM. The horizontal grid resolution is 3.125 km.

Metric	reference setup	no bed thermal model
number of surges	35 ± 25	20.7 ± 140.5
mean period	10 ± 10 kyr	79.9 ± 80.0
mean duration	3 ± 2 kyr	69.8 ± 60.4
mean ice volume change	$1.1 \pm 0.3 \cdot 10^5$ km^3	395.8 ± 240.5
RMSE	-	36.0 ± 5.3
Mean Bias	-	-27.1 ± 5.6

Table S8. Percentage differences (except first column) of surge characteristics, ice volume RMSE and mean bias compared to the PISM reference setup for runs without a bed thermal model. No runs crashed and all runs had more than 1 surge. The first 20 kyr of each run are treated as a spin-up interval for the surge characteristics (not the RMSE and mean bias).

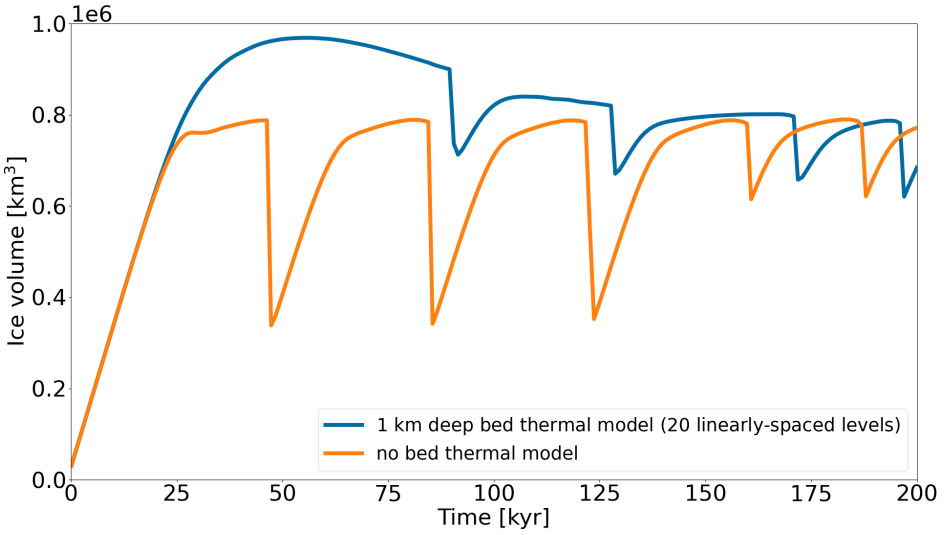

Figure S22. Ice volume in the eastern half of the pseudo-Hudson Bay and the pseudo-Hudson Strait for parameter vector 8 with and without the 1 km deep (20 linearly-spaced levels) bed thermal model using PISM. The horizontal grid resolution is 25 km.

S7.2 Basal-temperature at the grid cell interface

Metric	reference setup (TpmTrans)	TpmInt	TpmInt, upwind	TpmCen
nC	0	0	0	1
nS0	0	4	1	0
nS1	0	0	1	0
number of surges	180 ± 100	-96.9 ± 6.3	-90.2 ± 15.4	-74.6 ± 13.9
mean period	1.1 ± 0.5 kyr	106.2 ± 0.0	1645.4 ± 2136.8	609.4 ± 832.22
mean duration	0.3 ± 0.1 kyr	-15.9 ± 0.0	11.1 ± 17.4	43.3 ± 71.1
mean pseudo-Hudson Strait ice volume change	$1.7 \pm 0.2 \cdot 10^3$ km^3	-66.2 ± 0.0	-60.4 ± 6.5	-61.3 ± 5.6
RMSE	-	7.4 ± 2.4	9.4 ± 2.6	6.9 ± 2.5
Mean Bias	-	4.0 ± 1.6	6.7 ± 2.4	2.1 ± 2.1

Table S9. Percentage differences (except first column) of surge characteristics, pseudo-Hudson Strait ice volume RMSE and mean bias compared to the GSM reference setup for different approaches to calculate the basal-temperature at the grid cell interface (Sec. 3.3.2). Crashed runs (nC) are not considered and runs without surges (nS0) only contribute to the change in surge number. Runs with only 1 surge (nS1) are excluded from the calculation of the mean period. The first 20 kyr of each run are treated as a spin-up interval for the surge characteristics (not the RMSE and mean bias).

S7.3 Basal-temperature ramps at different resolutions

To simplify the comparison of different temperature ramps, we calculate a single value score based on all surge characteristics. The calculation steps are as follows.

1. calculate the absolute values for all surge characteristic means
2. calculate the average across all ramps for all characteristics (means and standard deviations separately, total of 4 means and 4 standard deviations)
3. for each ramp, divide all surge characteristics by their corresponding average
4. sum the values for all surge characteristics (separately for mean and std)

The above calculation combines the 4 surge characteristics to a single value for the mean and standard deviation of each ramp. We keep separate values for the mean and standard deviation since the two metrics contain different information. Smaller values indicate a better agreement with the 3.125 km reference setup.

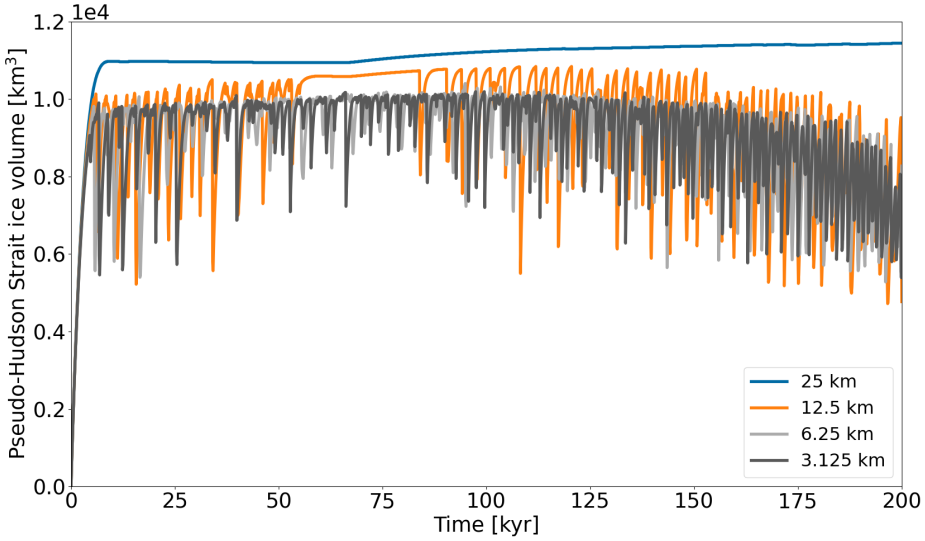

Figure S23. Pseudo-Hudson Strait ice volume for parameter vector 1 and different horizontal grid resolutions using the GSM. A constant temperature ramp with $T_{\mathrm{ramp}} = 0.0625^{\circ}\mathrm{C}$ and $T_{\mathrm{exp}} = 28$ is used for all horizontal grid resolutions (magenta line in Fig. 2).

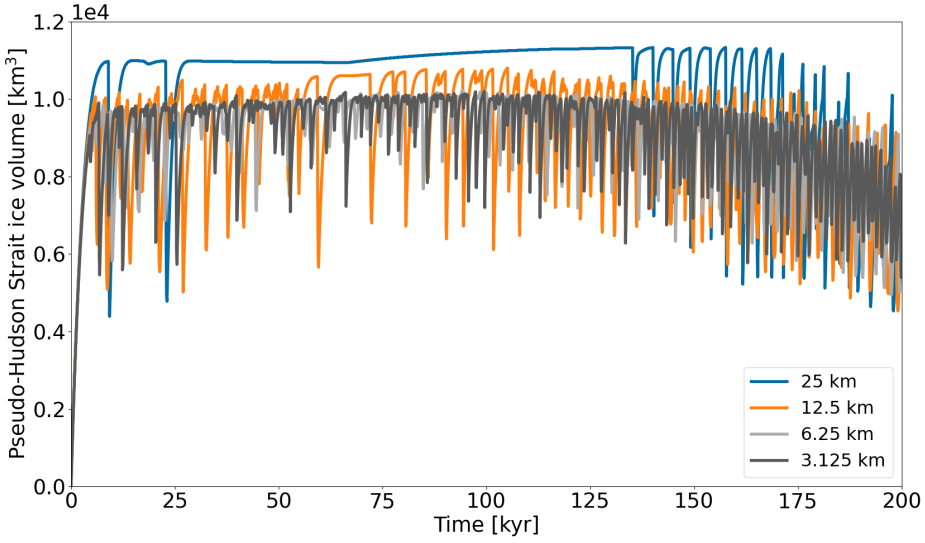

Figure S24. Pseudo-Hudson Strait ice volume for parameter vector 1 and different horizontal grid resolutions using the GSM. A resolution-dependent temperature (Eq. (9)) with $P_{\mathrm{T_{ramp}}} = 1$ and $T_{\mathrm{exp}} = 28$ is used for all horizontal grid resolutions (matching colors in Fig. 2).

Metric	#Surges	mean period	mean duration	mean pseudo-Hudson Strait ice volume change	RMSE	Mean Bias
$T_{\mathrm{exp}} = 5$, $T_{\mathrm{ramp}} = 1$	-63.5 ± 17.1	121.7 ± 29.5	300.0 ± 116.6	95.5 ± 39.5	21.8 ± 4.8	-17.8 ± 5.6
$T_{\mathrm{exp}} = 15$, $T_{\mathrm{ramp}} = 1$	-39.0 ± 10.2	64.6 ± 22.8	179.2 ± 117.3	51.5 ± 35.3	17.4 ± 3.7	-11.2 ± 4.6
$T_{\mathrm{exp}} = 28$, $T_{\mathrm{ramp}} = 0.5$	-17.1 ± 7.1	28.6 ± 21.0	64.0 ± 54.1	18.7 ± 12.4	10.0 ± 3.3	-3.5 ± 3.2
$T_{\mathrm{exp}} = 5$, $T_{\mathrm{ramp}} = 0.0625$	-9.5 ± 5.1	16.5 ± 12.4	14.9 ± 12.0	3.9 ± 2.9	8.1 ± 2.4	-0.8 ± 0.6
$T_{\mathrm{exp}} = 10$, $T_{\mathrm{ramp}} = 0.0625$	-9.3 ± 5.0	10.1 ± 5.0	8.8 ± 7.0	3.4 ± 4.0	8.0 ± 2.4	-0.4 ± 0.3
$T_{\mathrm{exp}} = 28$, $T_{\mathrm{ramp}} = 0.125$	-4.6 ± 6.4	3.2 ± 4.2	4.4 ± 5.4	0.3 ± 2.1	7.9 ± 2.2	-0.3 ± 0.2
$T_{\mathrm{exp}} = 14$, $T_{\mathrm{ramp}} = 0.0625$	-7.1 ± 5.1	9.3 ± 7.4	7.3 ± 7.5	2.8 ± 3.4	7.8 ± 1.9	-0.2 ± 0.1
$T_{\mathrm{exp}} = 15$, $T_{\mathrm{ramp}} = 0.0625$	-4.9 ± 4.7	8.4 ± 10.5	4.8 ± 4.4	0.3 ± 6.3	7.8 ± 2.0	-0.2 ± 0.1
$T_{\mathrm{exp}} = 20$, $T_{\mathrm{ramp}} = 0.0625$	-3.0 ± 4.7	2.0 ± 3.9	-0.1 ± 2.9	1.3 ± 4.2	7.9 ± 2.4	-0.1 ± 0.1
$T_{\mathrm{exp}} = 25$, $T_{\mathrm{ramp}} = 0.0625$	-1.2 ± 3.5	4.1 ± 7.7	0.5 ± 1.1	-1.5 ± 3.0	7.8 ± 2.4	-0.0 ± 0.1
3.125 km reference setup	$\mathbf{180 \pm 100}$	$\mathbf{1.1 \pm 0.5}$ **kyr**	$\mathbf{0.3 \pm 0.1}$ **kyr**	$\mathbf{1.7 \pm 0.2 \cdot 10^3}$ **km^3**	**-**	**-**
$T_{\mathrm{exp}} = 30$, $T_{\mathrm{ramp}} = 0.0625$	-2.4 ± 3.6	2.4 ± 3.9	-0.1 ± 2.9	-0.4 ± 2.4	7.9 ± 2.2	0.0 ± 0.1
$T_{\mathrm{exp}} = 35$, $T_{\mathrm{ramp}} = 0.0625$	-2.6 ± 4.7	2.6 ± 4.8	0.5 ± 4.3	-0.6 ± 4.1	7.9 ± 2.3	0.1 ± 0.2
$T_{\mathrm{exp}} = 45$, $T_{\mathrm{ramp}} = 0.0625$	-1.3 ± 4.8	1.8 ± 4.4	-0.1 ± 1.6	-1.6 ± 4.1	7.8 ± 2.2	0.1 ± 0.1
$T_{\mathrm{exp}} = 56$, $T_{\mathrm{ramp}} = 0.0625$	-1.7 ± 4.7	1.3 ± 4.7	-3.2 ± 2.1	-0.4 ± 5.2	7.7 ± 2.1	0.2 ± 0.0
$T_{\mathrm{exp}} = 28$, $T_{\mathrm{ramp}} = 0.03125$	-0.8 ± 4.9	3.2 ± 8.0	-2.3 ± 3.1	-0.2 ± 3.8	7.8 ± 2.3	0.2 ± 0.1

Table S10. Percentage differences (except for reference setup) of surge characteristics, pseudo-Hudson Strait ice volume RMSE and mean bias compared to the GSM reference setup ($T_{\mathrm{ramp}} = 0.0625$, $T_{\mathrm{exp}} = 28$) for different basal-temperature ramps. The ramps are sorted from widest (first row) to sharpest (last row, see Fig. S25). The bold reference values in the middle of the table separate the ramps that are wider (above) and sharper (below) than the reference setup. No runs crashed and all runs had more than 1 surge. The first 20 kyr of each run are treated as a spin-up interval for the surge characteristics (not the RMSE and mean bias).

ramp	score mean	score SD	sum of scores
res= 25 km, $T_{\mathrm{exp}} = 5$, $T_{\mathrm{ramp}} = 0.5$	**0.85**	**2.92**	**3.77**
res= 25 km, $T_{\mathrm{exp}} = 15$, $T_{\mathrm{ramp}} = 1$	1.08	3.53	4.61
res= 25 km, $T_{\mathrm{exp}} = 10$, $T_{\mathrm{ramp}} = 0.5$	1.58	3.88	5.46
res= 12.5 km, $T_{\mathrm{exp}} = 10$, $T_{\mathrm{ramp}} = 0.25$	3.87	4.11	7.98
res= 12.5 km, $T_{\mathrm{exp}} = 20$, $T_{\mathrm{ramp}} = 0.25$	3.04	2.55	**5.59**
res= 12.5 km, $T_{\mathrm{exp}} = 25$, $T_{\mathrm{ramp}} = 0.25$	3.43	3.31	6.74
res= 12.5 km, $T_{\mathrm{exp}} = 28$, $T_{\mathrm{ramp}} = 0.25$	**2.93**	2.72	5.65
res= 12.5 km, $T_{\mathrm{exp}} = 30$, $T_{\mathrm{ramp}} = 0.25$	3.54	**2.45**	5.99
res= 12.5 km, $T_{\mathrm{exp}} = 35$, $T_{\mathrm{ramp}} = 0.25$	3.30	2.98	6.28
res= 12.5 km, $T_{\mathrm{exp}} = 45$, $T_{\mathrm{ramp}} = 0.25$	3.36	3.17	6.54
res= 12.5 km, $T_{\mathrm{exp}} = 28$, $T_{\mathrm{ramp}} = 0.0625$	3.40	2.87	6.27
res= 6.25 km, $T_{\mathrm{exp}} = 10$, $T_{\mathrm{ramp}} = 0.125$	2.73	1.69	4.42
res= 6.25 km, $T_{\mathrm{exp}} = 15$, $T_{\mathrm{ramp}} = 0.125$	2.13	**1.17**	**3.30**
res= 6.25 km, $T_{\mathrm{exp}} = 20$, $T_{\mathrm{ramp}} = 0.125$	1.92	2.98	4.90
res= 6.25 km, $T_{\mathrm{exp}} = 25$, $T_{\mathrm{ramp}} = 0.125$	2.09	2.35	4.44
res= 6.25 km, $T_{\mathrm{exp}} = 28$, $T_{\mathrm{ramp}} = 0.125$	2.05	2.10	4.15
res= 6.25 km, $T_{\mathrm{exp}} = 30$, $T_{\mathrm{ramp}} = 0.125$	1.95	1.63	3.58
res= 6.25 km, $T_{\mathrm{exp}} = 35$, $T_{\mathrm{ramp}} = 0.125$	1.94	1.66	3.60
res= 6.25 km, $T_{\mathrm{exp}} = 45$, $T_{\mathrm{ramp}} = 0.125$	**1.70**	2.67	4.37
res= 6.25 km, $T_{\mathrm{exp}} = 28$, $T_{\mathrm{ramp}} = 0.0625$	1.80	2.56	4.36

Table S11. Single value scores for the mean and standard deviation of the basal-temperature ramps. The temperature ramps are shown in Fig. S26. A total of 12, 13, and 13 ramps were tested at 25 km, 12.5 km, and 6.25 km horizontal grid resolution, respectively. Note that ramps whose sum (score mean + score SD) differ by more than 50 % from the minimum sum at the corresponding resolution are not listed here. The minimum scores for the mean, standard deviation, and sum at each resolution are marked as bold numbers. No runs crashed and all runs had more than 1 surge. Note that the sum of scores can be slightly off due to rounding (± 0.01).

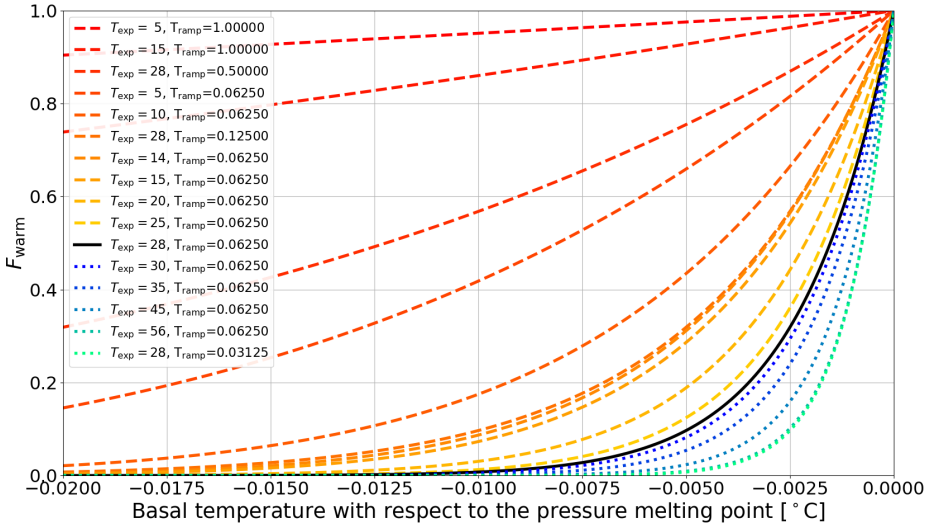

Figure S25. Temperature ramps for different values of T_{ramp} and T_{exp}. The black solid line shows the ramp used for the 3.125 km horizontal grid resolution reference setup ($T_{\mathrm{ramp}} = 0.0625$, $T_{\mathrm{exp}} = 28$). The solid and dotted lines show ramps that are wider and sharper than the reference setup, respectively. The depicted temperature ramps are the same as the ones listed in Fig. 9 and Table S10.

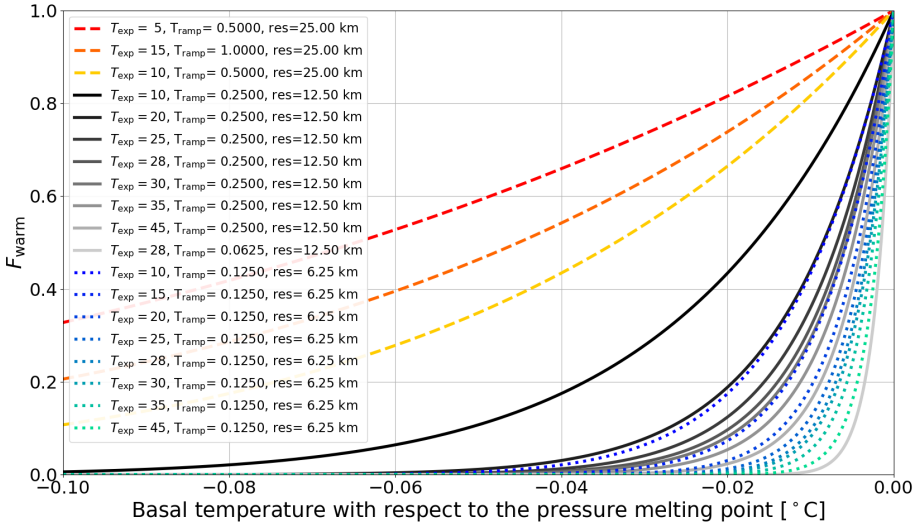

Figure S26. Shown are the temperature ramps listed in Table S11 at 25 km (dashed lines), 12.5 km (solid lines), and 6.25 km horizontal grid resolution (dotted lines).

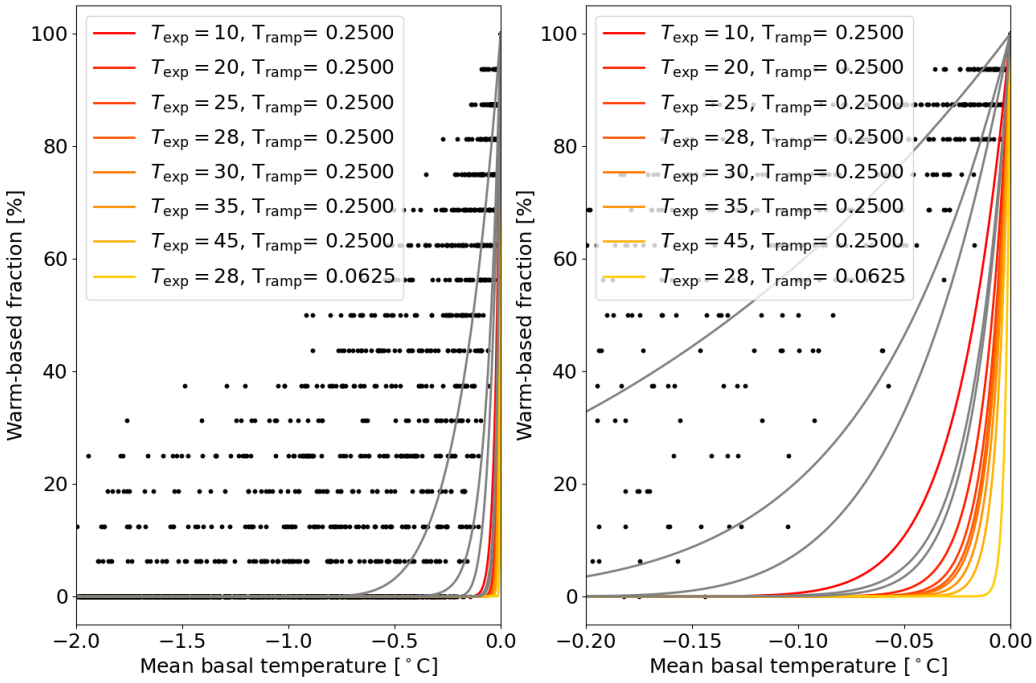

Figure S27. Warm-based fraction (basal-temperature with respect to the pressure-melting point at 0 °C) vs. mean basal-temperature with respect to the pressure-melting point when upscaling a 3.125 km run to 12.5 km horizontal grid resolution including all 5 parameter vectors using the GSM. Only grid cells within the pseudo-Hudson Strait and time steps within the surges of the 10 kyr after the first surge are considered. The restriction to the 10 kyr after the first surge for these experiments is set by storage limitations due to the high temporal resolution of the model output fields (10 yr). The colored ramps correspond to the 12.5 km horizontal grid resolution basal-temperature ramps in Table S11 and the gray lines show all other ramps that were tested at this resolution.

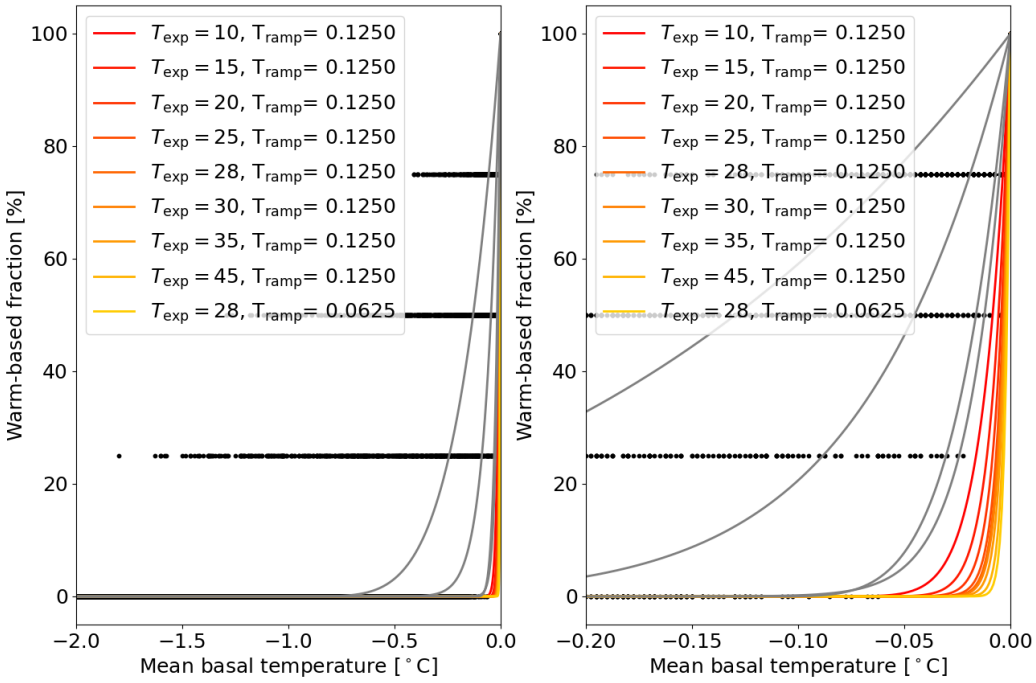

Figure S28. Warm-based fraction (basal-temperature with respect to the pressure-melting point at 0 °C) vs. mean basal-temperature with respect to the pressure-melting point when upscaling a 3.125 km run to 6.25 km horizontal grid resolution including all 5 parameter vectors using the GSM. The colored ramps correspond to the 6.25 km horizontal grid resolution basal-temperature ramps in Table S11 and the gray lines show all other ramps that were tested at this resolution. Otherwise same as Fig. S27.

S7.4 Smooth sediment transition zone and non-flat topography

Metric	reference setup (abrupt transition) reference values	3.125 km wide transition	25 km wide transition	3.125 km wide transition with HB/HS topography	25 km wide transition with HB/HS topography
number of surges	180 ± 100	-4.2 ± 8.9	1.0 ± 11.4	36.3 ± 17.3	19.9 ± 22.6
mean period	1.1 ± 0.5 kyr	4.6 ± 9.2	-0.4 ± 10.4	2.2 ± 48.0	14.5 ± 45.1
mean duration	0.3 ± 0.1 kyr	2.7 ± 3.6	7.2 ± 4.4	10.2 ± 17.5	24.3 ± 9.0
mean pseudo-Hudson Strait ice volume change	$1.7 \pm 0.2 \cdot 10^3$ km^3	0.2 ± 4.8	-1.7 ± 4.1	8.4 ± 10.0	17.3 ± 15.6
RMSE	-	7.9 ± 2.3	8.0 ± 2.2	11.2 ± 1.8	12.2 ± 2.0
Mean Bias	-	0.0 ± 0.2	-0.6 ± 0.5	-6.2 ± 1.9	-6.6 ± 2.2

Table S12. Percentage differences (except first column) of surge characteristics, pseudo-Hudson Strait ice volume RMSE and mean bias compared to the GSM reference setup for runs with a smooth transition between hard bedrock and soft sediment, and runs with a pseudo-Hudson Bay/Hudson Strait (HB/HS) topography. No runs crashed and all runs had more than 1 surge. The first 20 kyr of each run are treated as a spin-up interval for the surge characteristics (except for the RMSE and mean bias).

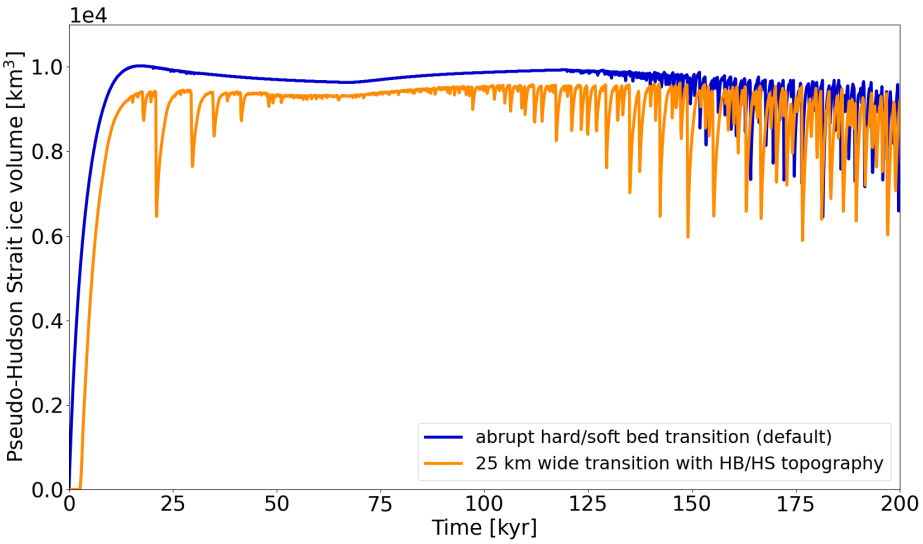

Figure S29. Pseudo-Hudson Strait ice volume for parameter vector 0 with and without a 200 m deep topography in the pseudo-Hudson Bay and Hudson Strait region using the GSM. In runs with a non-flat topography, the initial glaciation is delayed because the pseudo-Hudson Strait topography is below sea level. The horizontal grid resolution is 3.125 km.

Comparing the runs for parameter vector 1 more closely shows that when using a non-flat topography, the surges now start and propagate at the southernmost and northernmost end of the pseudo-Hudson Strait, where the topography is deepest and begins to slope upwards. Additionally, the surges tend to propagate faster and extend further to the West and in North-South direction than without topography (e.g., 8.0 to 8.3 kyr in the bottom row of video 07 of Hank (2023)). This is mainly due to

warmer basal conditions in the transition zone and Hudson Bay region before the start of the surge ($200\ \mathrm{m}$ bed depression increases the heat generation at the bed (video 08 of Hank (2023)) which, in turn, increases the average basal-temperature with respect to the pressure-melting point). Furthermore, the pressure-melting point in the $200\ \mathrm{m}$ deep Hudson Strait and $500\ \mathrm{m}$ deep ocean setup is first reached further inland and not at the eastern end of the pseudo-Hudson Strait, as is the case for a flat topography (e.g., 7.8 to $8.1\ \mathrm{kyr}$ in the bottom row of video 07 of Hank (2023)).

Metric	reference setup (smooth transition, e.g., Fig. S8) reference values	abrupt transition	smooth transition with HB/HS topography
number of surges	35 ± 25	-4.8 ± 13.4	-0.1 ± 190
mean period	10 ± 10 kyr	7.4 ± 24.5	79.0 ± 64.1
mean duration	3 ± 2 kyr	21.5 ± 59.4	56.2 ± 53.4
mean pseudo-Hudson Strait ice volume change	$1.1 \pm 0.3 \cdot 10^5\ \mathrm{km}^3$	14.1 ± 37.8	389.5 ± 169.8
RMSE	-	4.4 ± 2.5	37.7 ± 2.5
Mean Bias	-	-0.2 ± 0.3	-30.4 ± 1.4
nS0	0	0	3

Table S13. Percentage differences (except first column) of surge characteristics, ice volume RMSE and mean bias compared to the PISM reference setup for runs with an abrupt transition between hard bedrock and soft sediment, and runs with a pseudo-Hudson Bay/Hudson Strait (HB/HS) topography. No runs crashed and runs without surges (nS0) only contribute to the change in surge number. The first $20\ \mathrm{kyr}$ of each run are treated as a spin-up interval for the surge characteristics (except for the RMSE and mean bias).

S7.5 Basal-hydrology

Metric	no hydrology	local hydrology	no hydrology, double C_{rmu}	no hydrology, double C_{fslid}
number of surges	180 ± 100	-3.8 ± 23.8	-9.5 ± 3.9	-3.0 ± 8.8
mean period	1.1 ± 0.5 kyr	17.4 ± 44.9	12.4 ± 4.1	4.5 ± 10.3
mean duration	0.3 ± 0.1 kyr	11.6 ± 19.1	3.1 ± 5.6	2.3 ± 3.5
mean ice volume change	$1.7 \pm 0.2 \cdot 10^3\ \mathrm{km}^3$	20.2 ± 44.7	10.5 ± 5.9	-0.9 ± 5.8
RMSE	-	8.7 ± 2.6	8.5 ± 2.7	7.8 ± 2.2
Mean Bias	-	-0.9 ± 0.8	-0.4 ± 0.4	-0.1 ± 0.1

Table S14. Percentage differences (except first column) of surge characteristics, ice volume RMSE and mean bias of GSM runs with a local basal-hydrology model compared to runs without sub-glacial hydrology. Additionally shown are the changes in surge characteristics when doubling the values of the soft and hard-bed-sliding coefficient (C_{rmu} and C_{fslid} in Table 1, respectively). No runs crashed and all runs had more than 1 surge. The first $20\ \mathrm{kyr}$ of each run are treated as a spin-up interval for the surge characteristics (not the RMSE and mean bias).

S8 Sensitivity experiments without a significant effect

S8.1 Weight of adjacent minimum basal-temperature

Depending on the location of the adjacent minimum grid cell center basal-temperature, either the ice flow (when the adjacent minimum basal-temperature is downstream) or upstream propagation of the surge should be affected (decreasing basal interface temperature with increasing weight). For the large-scale surges, the adjacent minimum basal-temperature is almost exclusively located upstream (e.g., video 02 of Hank (2023)). Changing the weight of the adjacent minimum basal-temperature, therefore, affects the surge propagation rather than blocking parts of the ice flow.

Here we compare the effect of three different weights on the GSM surge characteristics (Eq. (S1)): no consideration of adjacent minimum basal-temperature ($W_{\mathrm{Tb,min}} = 0.0$), basal-temperature at the interface depends to $50\ \%$ on the adjacent minimum basal-temperature at the grid cell center (reference setup, $W_{\mathrm{Tb,min}} = 0.5$), and basal-temperature at the interface is equal to the adjacent minimum basal-temperature at the grid cell center ($W_{\mathrm{Tb,min}} = 1.0$).

Metric	reference setup	$W_{\mathrm{Tb,min}} = 0.0$	$W_{\mathrm{Tb,min}} = 1.0$
#Surges	180 ± 100	-9.6 ± 6.5	-3.7 ± 7.8
mean period	1.1 ± 0.5 kyr	14.7 ± 13.5	3.0 ± 0.8
mean duration	0.3 ± 0.1 kyr	5.1 ± 4.9	-2.6 ± 3.3
mean pseudo-Hudson Strait ice volume change	$1.7 \pm 0.2 \cdot 10^3$ km^3	-1.9 ± 4.0	4.0 ± 6.7
RMSE	-	7.8 ± 2.5	8.0 ± 2.5
Mean Bias	-	-0.1 ± 0.1	0.3 ± 0.1

Table S15. Percentage differences (except first column) of surge characteristics, pseudo-Hudson Strait ice volume RMSE and mean bias compared to the GSM reference setup ($W_{\mathrm{Tb,min}} = 0.5$) for different weights of the adjacent minimum basal-temperature for the basal-sliding temperature ramp. No runs crashed and all runs had more than 1 surge. The first 20 kyr of each run are treated as a spin-up interval for the surge characteristics (not the RMSE and mean bias).

The surge cycling response to changes in $W_{\mathrm{Tb,min}}$ is not coherent (Table S15). For instance, the mean surge period increases for both $W_{\mathrm{Tb,min}} = 0.$ and $W_{\mathrm{Tb,min}} = 1.0$ compared to the reference $W_{\mathrm{Tb,min}} = 0.5$. However, standard deviations are large, indicating a different model response for different parameter vectors.

S8.2 Different approaches to basal-hydrology

Here we compare the effects on surge characteristics when using a horizontal transport model in PISM instead of a simple local basal-hydrology. In general, PISM experiments with a mass-conserving horizontal transport hydrology model yield similar results to the local hydrology model (Fig. 7 and Table S16). The mean duration, period, and ice volume change increase ($11\ \%$, $10\ \%$, and $7\ \%$, respectively), while the number of surges decreases ($5\ \%$). These differences are on the same level as the MNEEs (Table 6) and show large standard deviations, indicating a different model response for different parameter vectors. The ice volume RMSE and mean bias are also small ($+3.9\ \%$ and $-0.1\ \%$, respectively).

S8.3 Basal-hydrology instead of basal-temperature ramp as the primary smoothing mechanism

We examine the effects of a local basal-hydrology as main smoothing mechanism for basal-sliding (compared to a basal-temperature ramp) by using a very sharp ramp ($T_{\mathrm{ramp}} = 0.001$, $T_{\mathrm{exp}} = 28$), minimizing the smoothing effect of the basal-temperature ramp. The change in surge characteristics between runs with local basal-hydrology and the sharp temperature ramp and the GSM reference setup is similar (maximum difference of $3\ \%$; compare Table S14 and S17) to the runs with local basal-hydrology and the reference basal-temperature ramp ($T_{\mathrm{ramp}} = 0.0625$, $T_{\mathrm{exp}} = 28$), indicating that the local basal-hydrology is the primary smoothing mechanism in both cases. The differences in the change of surge characteristics between the reference and the sharper ramp are smaller than the MNEEs, preventing further analysis.

Metric	local hydrology	horizontal transport
number of surges	35 ± 25	-4.6 ± 14.5
mean period	10 ± 10 kyr	10.8 ± 27.8
mean duration	3 ± 2 kyr	10.5 ± 35.4
mean ice volume change	$1.1 \pm 0.3 \cdot 10^5$ km^3	6.8 ± 17.9
RMSE	-	3.9 ± 2.5
Mean Bias	-	-0.1 ± 0.3

Table S16. Percentage differences (except first column) of surge characteristics, ice volume (eastern half of pseudo-Hudson Bay and the pseudo-Hudson Strait) RMSE and mean bias of PISM runs with a mass-conserving horizontal transport hydrology model compared to the local hydrology model. No runs crashed and all runs had more than 1 surge. The first 20 kyr of each run are treated as a spin-up interval for the surge characteristics (not the RMSE and mean bias).

Metric	reference setup	sharper ramp ($T_{\mathrm{ramp}} = 0.001$, $T_{\mathrm{exp}} = 28$), local hydrology
#Surges	180 ± 100	-3.8 ± 24.6
mean period	1.1 ± 0.5 kyr	16.0 ± 42.0
mean duration	0.3 ± 0.1 kyr	8.7 ± 17.0
mean pseudo-Hudson Strait ice volume change	$1.7 \pm 0.2 \cdot 10^3$ km^3	21.5 ± 43.3
RMSE	-	8.9 ± 3.2
Mean Bias	-	-0.6 ± 0.9

Table S17. Percentage differences (except first column) of surge characteristics, pseudo-Hudson Strait ice volume RMSE and mean bias compared to the GSM reference setup with local basal-hydrology instead of a basal-temperature ramp as the primary smoothing mechanism. No runs crashed and all runs had more than 1 surge. The first 20 kyr of each run are treated as a spin-up interval for the surge characteristics (not the RMSE and mean bias).

S9 Convergence study

S9.1 GSM convergence study without basal-hydrology

Analyzing individual GSM parameter vectors in detail shows that some discrepancies prevail even when using a resolution-dependent temperature ramp. In the case of parameter vector 1, for example, surges do still not occur for the coldest temperatures (Fig. S30). Note the asymmetry in termination and onset of surge cyclicity ($\Delta t_1 < \Delta t_2$). For increasing temperatures after the minimum surface temperature $T_{\mathrm{min}} = -15°\mathrm{C}$ at $t_{\mathrm{min}} = 66.7$ kyr, the first surge occurs at a surface temperature slightly higher than the initial temperature T_{init}, for which oscillations occur. The difference between Δt_1 and Δt_2 is ~ 25 kyr and closely resembles the lag of the average pseudo-Hudson Strait basal-temperature with respect to the pressure-melting point behind the surface temperature changes. For example, the minimum average pseudo-Hudson Strait basal-temperature with respect to the pressure-melting point ($T_{\mathrm{bpm}} = -3.2°\mathrm{C}$) occurs 23 kyr after the minimum surface temperature (not shown). The period without oscillations in the 25 km run corresponds to a period of somewhat smaller and less frequent oscillations in the finer resolution runs (Fig. S24).

Setup	number of surges	mean period	mean duration	mean pseudo-Hudson Strait ice volume change	nS0
3.125 km reference setup	180 ± 100	1.1 ± 0.5 kyr	0.3 ± 0.1 kyr	$1.7 \pm 0.2 \cdot 10^3$ km^3	0
25 km, constant ramp	-95.1 ± 7.4	942.3 ± 517.70	300.0 ± 172.22	95.9 ± 52.6	3
25 km, resolution-dependent ramp	-78.1 ± 18.2	414.5 ± 309.0	119.5 ± 17.6	91.9 ± 23.6	1
25 km, $T_{\text{ramp}} = 0.5$, $T_{\text{exp}} = 5$	-15.9 ± 20.4	29.7 ± 24.6	43.8 ± 36.6	3.5 ± 18.7	0
12.5 km, constant ramp	-59.2 ± 16.5	129.0 ± 41.8	90.3 ± 17.9	50.3 ± 76.5	0
12.5 km, resolution-dependent ramp, also minimum mean score	-56.5 ± 15.1	115.7 ± 46.8	101.1 ± 20.5	33.0 ± 66.3	0
6.25 km, constant ramp	-24.2 ± 13.1	36.4 ± 20.9	24.8 ± 8.5	14.9 ± 14.2	0
6.25 km, resolution-dependent ramp	-27.9 ± 9.9	42.2 ± 18.9	32.1 ± 6.3	15.9 ± 12.3	0
6.25 km, $T_{\text{ramp}} = 0.125$, $T_{\text{exp}} = 45$	-25.3 ± 13.6	37.9 ± 26.7	28.2 ± 7.0	9.8 ± 11.6	0

Table S18. Percentage differences (except first row) of surge characteristics compared to the 3.125 km GSM reference setup. The values represent the average of 5 parameter vectors. No runs crashed and runs without surges (nS0) only contribute to the change in surge numbers. The first 20 kyr of each run are treated as a spin-up interval and are not considered in the above. The resolution-dependent ramps ($T_{\text{exp}} = 28$) and constant ramp (black line, $T_{\text{ramp}} = 0.0625$, $T_{\text{exp}} = 28$) are shown in Fig. 2. The third ramp listed for each resolution is the ramp with the smallest mean score (Table S11).

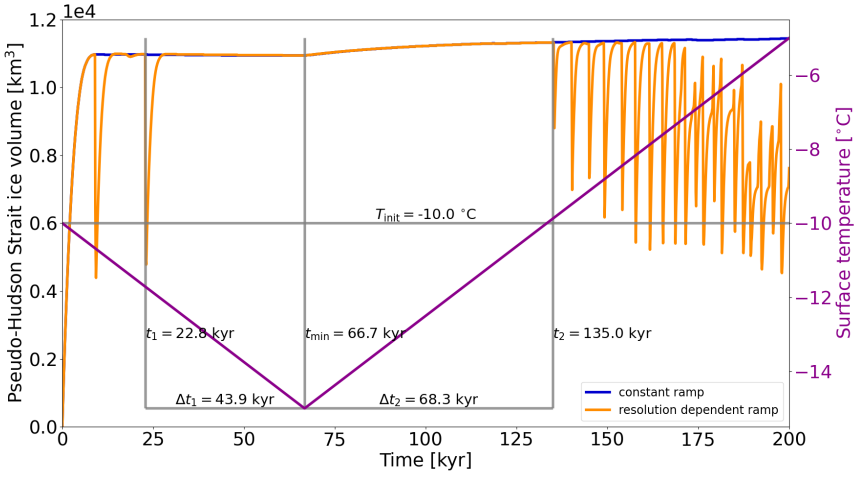

Figure S30. Pseudo-Hudson Strait ice volume for parameter vector 1 and different basal-temperature ramps using the GSM (constant ramp: $T_{\text{ramp}} = 0.0625°$C and $T_{\text{exp}} = 28$; resolution-dependent ramp: $T_{\text{ramp}} = 0.5°$C and $T_{\text{exp}} = 28$, see Fig. 2). The right axis shows the surface temperature when ignoring the lapse rate dependency. t_{min}, t_1, and t_2 mark the time of the minimum surface temperature, the start of the last surge before t_{min}, and the start of the first surge after t_{min}, respectively. Δt_1 and Δt_2 represent the time difference between t_{min} and t_1 and t_2, respectively. T_{init} indicates the surface temperature at the beginning of the run.

Setup	mean RMSE	mean Bias
25 km, constant ramp	17.1 ± 4.7	14.6 ± 4.4
12.5 km, constant ramp	10.3 ± 2.5	4.0 ± 1.1
6.25 km, constant ramp	8.7 ± 2.2	0.4 ± 0.5
25 km, resolution-dependent ramp	15.3 ± 3.0	10.3 ± 2.5
12.5 km, resolution-dependent ramp	10.3 ± 2.8	3.0 ± 2.3
6.25 km, resolution-dependent ramp	8.5 ± 2.3	0.2 ± 0.6
25 km, $T_{\mathrm{ramp}} = 0.5$, $T_{\mathrm{exp}} = 5$	12.8 ± 2.4	6.4 ± 1.7
12.5 km, $T_{\mathrm{ramp}} = 0.25$, $T_{\mathrm{exp}} = 28$, same as resolution-dependent ramp	10.3 ± 2.8	3.0 ± 2.3
6.25 km, $T_{\mathrm{ramp}} = 0.125$, $T_{\mathrm{exp}} = 45$	8.5 ± 2.0	0.6 ± 0.5

Table S19. Pseudo-Hudson Strait ice volume RMSE and mean bias compared to the 3.125 km GSM reference setup in percent. The values represent the average of 5 parameter vectors. No runs crashed and the entire 200 kyr run time is used (no spin-up interval).

S9.2 GSM convergence study with basal-hydrology

Based on the results without basal-hydrology (Sec. 3.4.1), 5 basal-temperature ramps ($T_{\mathrm{exp}} = [5, 10, 15, 20, 28]$) with a resolution-dependent T_{ramp} (Eq. (9)) are tested for all resolutions. As it is unclear which basal-temperature ramp should be used at the finest horizontal grid resolution (3.125 km), we test two different ramps ($T_{\mathrm{exp}} = [5, 28]$). The experiments that yield the smallest differences in surge characteristics (smallest mean score in Table S20 and S21) compared to the corresponding 3.125 km reference runs (bold rows) are presented in Table S22.

Similar to the results without a basal-hydrology model, the smallest differences in surge characteristics (except the mean pseudo-Hudson Strait ice volume change) occur for the coarsest horizontal grid resolution (25 km, Table S22). This likely indicates that the optimal ramps at 12.5 and 6.25 km horizontal grid resolution have not been found.

In general, the resolution-dependent ramp with $T_{\mathrm{exp}} = 5$ leads to the smallest differences between coarse- and fine-resolution runs. The differences in surge characteristics are significantly smaller than for a resolution-dependent temperature ramp without local basal-hydrology (except for the mean pseudo-Hudson Strait ice volume change, Table S18 vs. S22), further underlining the importance of the basal-hydrology.

Except for 12.5 km horizontal grid resolution, the resolution-dependent ramp with $T_{\mathrm{exp}} = 5$ yields a self-consistent response across all resolutions. At 12.5 km, the next closest exponent ($T_{\mathrm{exp}} = 10$) has the minimum mean score. However, given that there is no single best ramp across all resolutions, we assess different ramps as to whether differences are within inferred numerical errors (DWINE). To this end, we calculate the differences between the ramp with the minimum mean score and all other ramps at each resolution and for all surge characteristics (Table S20 and S21). We rule out ramps for which the differences exceed the maximum MNEEs (maximum of Table 5 and S2) for more than one surge characteristic (DWINE failures).

Under these criteria and when using $T_{\mathrm{exp}} = 5$ at 3.125 km horizontal grid resolution, the resolution-dependent ramp with $T_{\mathrm{exp}} = 10$ remains within the DWINE ensemble for all resolutions (Table S21). The results for $T_{\mathrm{exp}} = 28$ at 3.125 km horizontal grid resolution do not yield a single ramp that remains within the DWINE ensemble at all resolutions (Table S20). However, except for 6.25 km, for which the differences between the tested basal-temperature ramps are the smallest, $T_{\mathrm{exp}} = 5$ yields the minimum mean-score.

The pseudo-Hudson Strait ice volume RMSE and mean bias show convergence (smaller differences) for both 3.125 km horizontal grid resolution setups (Table S23).

ramp	score mean	score SD	sum of scores	DWINE failures
res= 25 km, $T_{\mathrm{exp}} = 5$, $T_{\mathrm{ramp}} = 0.5$	**0.99**	4.31	**5.31**	0
res= 25 km, $T_{\mathrm{exp}} = 10$, $T_{\mathrm{ramp}} = 0.5$	1.44	5.29	6.74	2
res= 25 km, $T_{\mathrm{exp}} = 15$, $T_{\mathrm{ramp}} = 0.5$	4.80	**3.05**	7.85	4
res= 25 km, $T_{\mathrm{exp}} = 20$, $T_{\mathrm{ramp}} = 0.5$	5.65	3.47	9.11	4
res= 25 km, $T_{\mathrm{exp}} = 28$, $T_{\mathrm{ramp}} = 0.5$	7.11	3.88	11.00	4
res= 12.5 km, $T_{\mathrm{exp}} = 5$, $T_{\mathrm{ramp}} = 0.25$	**3.69**	4.60	8.29	0
res= 12.5 km, $T_{\mathrm{exp}} = 10$, $T_{\mathrm{ramp}} = 0.25$	3.81	5.07	8.88	2
res= 12.5 km, $T_{\mathrm{exp}} = 15$, $T_{\mathrm{ramp}} = 0.25$	3.82	4.11	7.93	2
res= 12.5 km, $T_{\mathrm{exp}} = 20$, $T_{\mathrm{ramp}} = 0.25$	4.21	3.42	7.63	3
res= 12.5 km, $T_{\mathrm{exp}} = 28$, $T_{\mathrm{ramp}} = 0.25$	4.47	**2.81**	**7.28**	4
res= 6.25 km, $T_{\mathrm{exp}} = 5$, $T_{\mathrm{ramp}} = 0.125$	4.03	4.29	8.33	3
res= 6.25 km, $T_{\mathrm{exp}} = 10$, $T_{\mathrm{ramp}} = 0.125$	3.94	**3.76**	7.70	3
res= 6.25 km, $T_{\mathrm{exp}} = 15$, $T_{\mathrm{ramp}} = 0.125$	4.65	3.90	8.55	1
res= 6.25 km, $T_{\mathrm{exp}} = 20$, $T_{\mathrm{ramp}} = 0.125$	3.79	3.82	**7.60**	1
res= 6.25 km, $T_{\mathrm{exp}} = 28$, $T_{\mathrm{ramp}} = 0.125$	**3.59**	4.23	7.82	0

Table S20. Single value scores for the mean and standard deviation of the basal-temperature ramps and the number of DWINE failures (maximum 4) for a resolution-dependent reference temperature ramp with $T_{\mathrm{exp}} = 28$ in the GSM. The minimum scores for the mean, standard deviation, and sum at each resolution are marked as bold numbers. At $= 25$ km, 1 run crashed for $T_{\mathrm{exp}} = 10$ and 1 run showed no surges for $T_{\mathrm{exp}} = [15, 20, 28]$. Note that the sum of scores can be slightly off due to rounding (± 0.01).

ramp	score mean	score SD	sum of scores	DWINE failures
res= 25 km, $T_{\mathrm{exp}} = 5$, $T_{\mathrm{ramp}} = 0.5$	**0.84**	3.91	**4.75**	0
res= 25 km, $T_{\mathrm{exp}} = 10$, $T_{\mathrm{ramp}} = 0.5$	1.21	5.04	6.25	1
res= 25 km, $T_{\mathrm{exp}} = 15$, $T_{\mathrm{ramp}} = 0.5$	4.89	**3.29**	8.18	4
res= 25 km, $T_{\mathrm{exp}} = 20$, $T_{\mathrm{ramp}} = 0.5$	5.76	3.63	9.40	4
res= 25 km, $T_{\mathrm{exp}} = 28$, $T_{\mathrm{ramp}} = 0.5$	7.30	4.13	11.43	4
res= 12.5 km, $T_{\mathrm{exp}} = 5$, $T_{\mathrm{ramp}} = 0.25$	3.97	4.49	8.45	2
res= 12.5 km, $T_{\mathrm{exp}} = 10$, $T_{\mathrm{ramp}} = 0.25$	**3.77**	4.60	8.37	0
res= 12.5 km, $T_{\mathrm{exp}} = 15$, $T_{\mathrm{ramp}} = 0.25$	3.79	4.13	7.93	1
res= 12.5 km, $T_{\mathrm{exp}} = 20$, $T_{\mathrm{ramp}} = 0.25$	4.10	3.50	**7.59**	1
res= 12.5 km, $T_{\mathrm{exp}} = 28$, $T_{\mathrm{ramp}} = 0.25$	4.37	**3.28**	7.65	2
res= 6.25 km, $T_{\mathrm{exp}} = 5$, $T_{\mathrm{ramp}} = 0.125$	**3.53**	4.44	7.97	0
res= 6.25 km, $T_{\mathrm{exp}} = 10$, $T_{\mathrm{ramp}} = 0.125$	4.27	3.77	8.04	0
res= 6.25 km, $T_{\mathrm{exp}} = 15$, $T_{\mathrm{ramp}} = 0.125$	4.59	3.82	8.42	1
res= 6.25 km, $T_{\mathrm{exp}} = 20$, $T_{\mathrm{ramp}} = 0.125$	3.91	**3.64**	**7.55**	1
res= 6.25 km, $T_{\mathrm{exp}} = 28$, $T_{\mathrm{ramp}} = 0.125$	3.70	4.33	8.03	3

Table S21. Single value scores for the mean and standard deviation of the basal-temperature ramps and the number of DWINE failures (maximum 4) for a resolution-dependent reference temperature ramp with $T_{\mathrm{exp}} = 5$ in the GSM. The minimum scores for the mean, standard deviation, and sum at each resolution are marked as bold numbers. At $= 25$ km, 1 run crashed for $T_{\mathrm{exp}} = 10$ and 1 run showed no surges for $T_{\mathrm{exp}} = [15, 20, 28]$. Note that the sum of scores can be slightly off due to rounding (± 0.01).

Setup	number of surges	mean period	mean duration	mean pseudo-Hudson Strait ice volume change
3.125 km, $T_{\mathrm{ramp}} = 0.0625$, $T_{\mathrm{exp}} = 28$	$\mathbf{197 \pm 131}$	$\mathbf{1.5 \pm 1.1}$ **kyr**	$\mathbf{0.3 \pm 0.2}$ **kyr**	$\mathbf{2.0 \pm 0.7 \cdot 10^3}$ **km^3**
25 km, $T_{\mathrm{ramp}} = 0.5$, $T_{\mathrm{exp}} = 5$	9.7 ± 59.9	15.5 ± 42.3	24.3 ± 36.1	13.6 ± 46.7
12.5 km, $T_{\mathrm{ramp}} = 0.25$, $T_{\mathrm{exp}} = 5$	-36.1 ± 17.6	68.0 ± 49.8	97.1 ± 60.3	3.0 ± 26.4
6.25 km, $T_{\mathrm{ramp}} = 0.125$, $T_{\mathrm{exp}} = 28$	-13.2 ± 31.1	27.0 ± 40.6	25.7 ± 25.2	5.6 ± 27.5
3.125 km, $T_{\mathrm{ramp}} = 0.0625$, $T_{\mathrm{exp}} = 5$	$\mathbf{190 \pm 118}$	$\mathbf{1.3 \pm 0.7}$ **kyr**	$\mathbf{0.3 \pm 0.2}$ **kyr**	$\mathbf{1.8 \pm 0.4 \cdot 10^3}$ **km^3**
25 km, $T_{\mathrm{ramp}} = 0.5$, $T_{\mathrm{exp}} = 5$	-2.4 ± 35.8	16.1 ± 31.4	20.7 ± 30.3	14.3 ± 35.8
12.5 km, $T_{\mathrm{ramp}} = 0.25$, $T_{\mathrm{exp}} = 10$	-37.7 ± 12.1	61.7 ± 44.1	63.4 ± 34.8	20.5 ± 39.0
6.25 km, $T_{\mathrm{ramp}} = 0.125$, $T_{\mathrm{exp}} = 5$	-25.6 ± 13.9	37.8 ± 23.8	41.1 ± 21.3	0.3 ± 19.8

Table S22. Percentage differences (except bold rows) of surge characteristics compared to the 3.125 km GSM setups with local basal-hydrology (bold rows, $T_{\mathrm{exp}} = [5, 28]$) for the ramps with the smallest mean score (analysis steps described in Sec. S7.3). The values represent the average of 5 parameter vectors. No runs crashed and all runs had more than 1 surge. The first 20 kyr of each run are treated as a spin-up interval and are not considered in the above.

Setup	mean RMSE	mean Bias
25 km, $T_{\mathrm{ramp}} = 0.5$, $T_{\mathrm{exp}} = 5$	14.3 ± 3.2	6.0 ± 0.9
12.5 km, $T_{\mathrm{ramp}} = 0.25$, $T_{\mathrm{exp}} = 5$	11.2 ± 4.2	0.6 ± 2.4
6.25 km, $T_{\mathrm{ramp}} = 0.125$, $T_{\mathrm{exp}} = 28$	10.0 ± 3.0	0.5 ± 0.6
25 km, $T_{\mathrm{ramp}} = 0.5$, $T_{\mathrm{exp}} = 5$	14.5 ± 3.2	6.8 ± 0.4
12.5 km, $T_{\mathrm{ramp}} = 0.25$, $T_{\mathrm{exp}} = 10$	11.7 ± 4.2	1.6 ± 2.5
6.25 km, $T_{\mathrm{ramp}} = 0.125$, $T_{\mathrm{exp}} = 5$	10.1 ± 1.8	0.6 ± 0.8

Table S23. Resolution scaling of pseudo-Hudson Strait ice volume RMSE and mean bias with local basal-hydrology in percent. The three upper ramps are compared to the 3.125 km GSM setup with $T_{\mathrm{exp}} = 28$, the lower three to $T_{\mathrm{exp}} = 5$. The values represent the average of 5 parameter vectors. No runs crashed and the entire 200 kyr run time is used (no spin-up interval).

S9.3 GSM convergence study with active SSA everywhere (no basal-hydrology)

Setup	number of surges	mean period	mean duration	mean pseudo-Hudson Strait ice volume change	nS0
3.125 km reference setup	216 ± 146	1.3 ± 0.8 kyr	0.3 ± 0.1 kyr	$1.4 \pm 0.6 \cdot 10^3$ km^3	0
25 km	-76.9 ± 17.9	432.2 ± 384.3	151.7 ± 49.0	163.8 ± 65.9	1
12.5 km	-61.3 ± 23.8	179.8 ± 127.1	154.3 ± 79.3	40.1 ± 54.4	0
6.25 km	-46.2 ± 11.6	66.7 ± 12.9	59.8 ± 19.5	75.1 ± 42.9	0

Table S24. Percentage differences (except first row) of surge characteristics compared to the 3.125 km GSM reference setup with a resolution-dependent basal-temperature ramp ($T_{\mathrm{exp}} = 28$, Fig. 2) and active SSA everywhere. The values represent the average of 5 parameter vectors. No runs crashed and runs without surges (nS0) only contribute to the change in surge numbers. The first 20 kyr of each run are treated as a spin-up interval and are not considered in the above.

S9.4 PISM convergence study

195 Similar to the results presented for the GSM (Sec. S9.1 and S9.2), analyzing individual parameter vectors for PISM shows significant differences in surge behavior for different horizontal grid resolutions. Parameter vector 8 at 25 km horizontal grid resolution, for example, only shows 4 oscillations (Fig. S31). In contrast, more oscillations occur for both the 12.5 km and 50 km horizontal grid resolution run. Additionally, most of the 50 km surges transport ice toward the West, whereas the 25 and 12.5 km runs almost exclusively surge through the pseudo-Hudson Strait (video 09 of Hank (2023)).

Setup	number of surges	mean period	mean duration	mean ice volume change	nC	nS0	nS1
12.5 km reference setup	$\mathbf{22 \pm 19}$	$\mathbf{9 \pm 6}$ **kyr**	$\mathbf{3 \pm 1}$ **kyr**	$\mathbf{1.3 \pm 0.2 \cdot 10^5}$ **km^3**	**4**	**1**	**0**
50 km	4.1 ± 46.0	15.3 ± 47.4	11.9 ± 33.7	30.6 ± 39.6	0	0	1
25 km	-28.3 ± 12.0	46.5 ± 31.9	6.3 ± 13.8	4.0 ± 20.3	0	0	0

Table S25. Percentage differences (except bold row) of PISM surge characteristics due to different horizontal grid resolutions. Note that the 12.5 km (finest resolution tested) is used as a reference for the grid resolution convergence study. 4 of the 12.5 km runs crashed after $\sim$ 50 kyr because they hit the run-time limit on the computational cluster (7 days) and one 12.5 km run does not show a surge (nS0). Crashed runs (nC) are not considered and runs without surges in the comparison setup only contribute to the change in surge numbers. Runs without surges in the reference setup are not considered. The first 20 kyr of each run are treated as a spin-up interval and are not considered in the above.

Setup	nC	mean RMSE	mean Bias
50 km	0	11.1 ± 2.6	6.5 ± 4.1
25 km	0	7.4 ± 1.4	3.7 ± 0.8

Table S26. Ice volume RMSE and mean bias (in percent) due to different horizontal grid resolutions. Note that the 12.5 km (finest resolution tested) is used as a reference for the grid resolution convergence study. 4 of the 12.5 km runs crashed after $\sim$ 50 kyr because they hit the run-time limit on the computational cluster (7 days) and one 12.5 km run does not show a surge (nS0). Crashed runs (nC) are not considered. The entire 200 kyr run time is used (no spin-up interval).

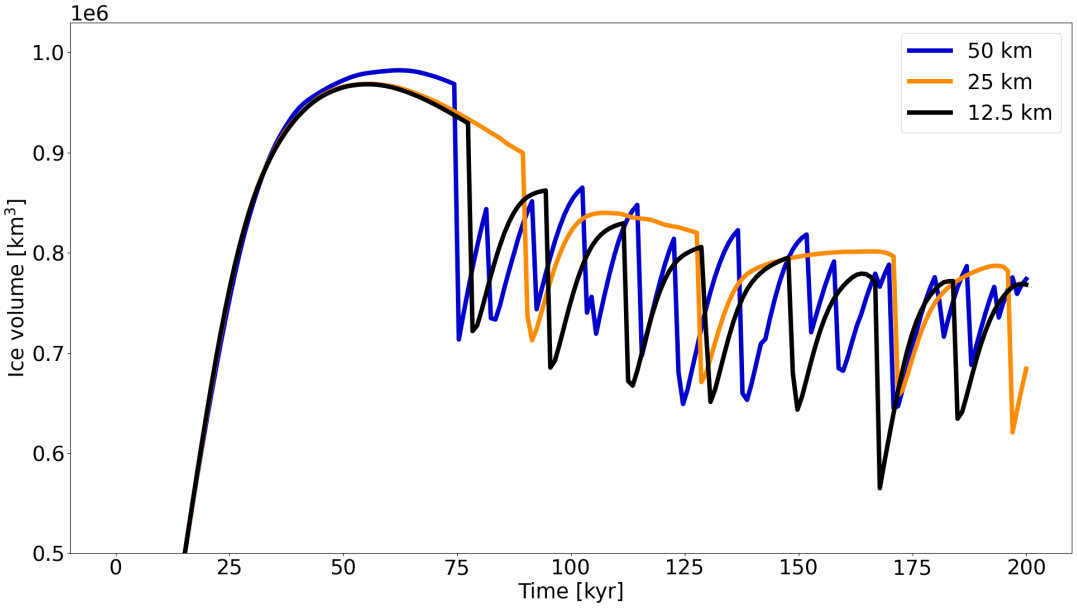

Figure S31. Ice Volume in the eastern half of the pseudo-Hudson Bay and the pseudo-Hudson Strait for parameter vector 8 and different horizontal grid resolutions using PISM. See also video 09 of Hank (2023).

References

Bueler, E. and Van Pelt, W.: Mass-conserving subglacial hydrology in the Parallel Ice Sheet Model version 0.6, Geoscientific Model Development, 8, 1613–1635, https://doi.org/10.5194/gmd-8-1613-2015, 2015.

Hank, K.: Supplementary material for "Numerical issues in modeling thermally and hydraulically driven ice stream surge cycling", https://doi.org/10.5281/zenodo.7905404, 2023.

K.M. Cuffey and W.S.B. Paterson.: The Physics of Glaciers, Butterworth-Heinemann/Elsevier, Burlington, MA, 4th edn., 2010.

Mitchell, J. and Soga, K.: Fundamentals of Soil Behavior, John Wiley & Sons, Inc., 3ed edn., 2005.

Sauer, E. K., Egeland, A. K., and Christiansen, E. A.: Preconsolidation of tills and intertill clays by glacial loading in southern Saskatchewan, Canada, Canadian Journal of Earth Sciences, 30, 420–433, https://doi.org/10.1139/e93-031, 1993.

Tulaczyk, S., Kamb, W. B., and Engelhardt, H. F.: Basal mechanics of Ice Stream B, West Antarctica 1. Till mechanics, Journal of Geophysical Research: Solid Earth, 105, 463–481, https://doi.org/10.1029/1999jb900329, 2000.